UNIVERSITY OF TWENTE – INORGANIC MEMBRANES

Hybrid polyPOSS-amide Membranes for Nanofiltration

Bachelor Assignment

Lynn Maria Schneider

23/6/2014

Examination Committee

Prof. Dr. ir. N.E Benes

Dr. ir. H. Wormeester

Ir. M. J. T. Raaijmakers

Ir. E. Maaskant

Dr. ir. W. Ogieglo

ABSTRACT

There is a lack of positively charged nanofiltration (NF) membranes which enable the removal of multivalent cations such as toxic dyes, calcium or heavy metals from industrial effluents. Positively charged NF membranes are promising to improve both, separation performance and energy efficiency compared to common separation techniques used. [1] In this study, hybrid inorganic-organic polyamide NF membranes were synthesized and investigated with respect to their positive charge behavior. The hybrid and hyper-crosslinked nature of these membranes offers outstanding thermal-mechanical stability. The membranes were synthesized by interfacial polymerization of octa-ammonium polyhedral oligomeric silsesquioxane (POSS) and isophtaloyl dichloride. For the polycondensation reaction POSS molecules were activated by converting unreactive ammonium groups to primary amine groups with addition of sodium hydroxide. The concept was to change the pH of the POSS solution in the synthesis and study the effect on charge and cross-linking. Characterization by attenuated total reflection infrared spectroscopy and x-ray photoelectron spectroscopy showed a trend of more positive charges for lower preparation pH and similarly more cross-linking for membranes with higher pH values. Streaming Zeta potential measurements showed isoelectric points around 8 for all membranes; indicating that all synthesized membranes were positively charged below pH 8 and that a low amount of carboxylic acid groups was present.

LIST OF ABBREVIATIONS AND SYMBOLS

AFM	atomic force microscopy
ATR-FT-IR	attenuated total reflectance- Fourier tansform- Infrared
BHAC	hexafunctional 2,2′,4,4′,6,6′-biphenyl hexaacyl chloride
CI	confidence interval
ELD	electric double layer
HS	Helmholtz and Smoluchowski
IDC	isophthaloyl dichloride
IEP	isoelectric point
IP	interfacial polymerization
IR	infrared
KCl	potassium chloride
NF	nanofiltration
PAN	polyacrylnitrile
PIP	piperazine
POSS	polyhedral oligomeric silsesquioxane
RO	reverse osmosis
SDS	sodium dodecyl sulphate
SEM	scanning electron microscopy
TFC	thin film composite
TMC	trimesoyl chloride
XPS	X-ray photoelectron spectroscopy

A	cross-sectional area of cell block
C_p	concentration of permeate
C_R	concentration of retentate
d_{ionh}	diameter of hydrated ions
dP	change in pressure
d_p	diameter of membrane pores
dU_s	change in streaming potential
h	Planck's constant
L	cell length
pka	dissociation constant
R	retention
R	cell resistance
v	frequency
α	separation factor
ε	dielectric constant of the electrolyte
ε_0	vacuum permittivity
ζ	zeta potential
η	electrolyte viscosity

TABLE OF CONTENTS

1. INTRODUCTION

Membranes are widely used, especially for waste water treatment. 40 % of membranes are applied in the production of ultrapure water for electronics, pharmaceutical and power generation industries whereas the remainder is applied in food and textile industry. [2] A membrane is a semi-permeable barrier, separating two or more species by having a higher permeability towards one component than the others. They often provide high energy efficiencies since separation is mostly based on transport rates instead of e.g. relative volatility (distillation). Most membranes consist of polymeric materials. Accordingly, membranes are versatile since their characteristics are adjustable. Nevertheless, polymeric materials often suffer from chemical instability and swelling in solvents. [2] The main challenges in membrane technology are lifetime, fouling issues, swelling and operational or material costs. [3] This thesis focuses on pressure driven membranes, particularly nanofiltration (NF) membranes for liquid-liquid separation since they are foreseen to have a promising market potential [4].

Separation by size exclusion plays a minor role in NF compared to membrane-solute interactions. [5] In NF membranes, charges have a large impact on rejection of ions and charged molecules as well as fouling properties. Most NF membranes are neutrally or negatively charged when processing in aqueous environment due to undesired side-reactions. [2] Positively charged membranes provide good hydrophilicity and high rejections of multivalent cations e.g. Mg^{2+}, Ca^{2+} [6] or dyes and heavy metals [6], [1]. Exhibiting those properties, positively charged membranes are important for recovery of valuable cationic macro-molecules in the bioprocess and pharmaceutical industries. In addition, they are promising for application in paper and pulp, textiles, nuclear, and automotive industries. Wastewater from the textile industries is one of major pollution sources from the industrial sector and entails severe environmental problems for several decades. Positively charged membranes would be greatly applicable for the removal of toxic dyes. Current technologies such as adsorption, photo-catalysis and enzymatic decomposition have proved to be highly inefficient for the removal of dyes form textile wastewaters. Positively charged membranes are promising to reduce costs and to improve separation performance. [1]

Interfacial polymerization (IP) is a versatile technique to produce NF membranes. Wang et al [7] produced positively charged TFC membranes by IP. The hyper cross-linked polyamide membranes were produced from hexafunctional 2,2′,4,4′,6,6′-biphenyl hexaacyl chloride (BHAC) and piperazine (PIP). According to their study, the high diffusivity of PIP molecules in the opposite phase led to a larger number of amine groups on the membrane surface. The amine groups are characteristic for the positive charges (isoelectric point ~pH 10). [7] Other approaches to create positive charges on membranes are surface grafting modification (quaternation) [8], coating [9] and blending [10], [11]. As a matter of fact, there is a lack of positively charged NF membranes for commercial and laboratory uses. Recently, studies have been dedicated to preparation, characterization and application of positively charged membranes.

The goal of this research was to systematically influence the behavior of positive charges and study the degree of polymerization of hybrid polyhedral oligomeric silsesquioxane (POSS) polyamide membranes. Research by Dalwani et al [4] showed that hybrid membranes own high thermal-mechanical stability since they comprise organic and inorganic components. In this work, five polyPOSS amide membranes were synthesized by IP on a porous polyacrylnitrile (PAN) support. Octa-ammonium POSS (Chapter 2.1.2, Figure 4) and isophthaloyl dichloride (IDC) (Chapter 2.1.2, Figure 5) were the monomers used in the IP synthesis. Before the IP reaction was promoted, the unreactive

ammonia groups of the POSS cage were converted to primary amine groups by changing the pH of the POSS solution with sodium hydroxide (NaOH). The hypothesis is that lower pH should reduce amount of converted ammonia groups of POSS cages; leading to more positively charged ammonia groups remaining on the membranes. Similarly, with increasing pH values of the POSS- solution, more reactive amine groups are present and thus the cross-linking of the membrane is higher. For analysis of these hypotheses, five membranes with pH varying from pH 8.3-9.9 were fabricated and discussed by means of different characterization methods. Attenuated total reflectance Fourier transform infrared spectroscopy (ATR-FT-IR) and X-ray photoelectron spectroscopy (XPS) have provided information about bulk and surface chemical composition and oxidation states of the groups on the surface. Streaming zeta potential measurements and contact angle titration were intended to provide information about surface charges. Additionally, contact angles have given an indication of the hydrophilicity of membranes.

The thesis is built up in the following manner: First there is a theoretical chapter, explaining aspects of NF membranes such as materials, synthesis method, and charge effect on molecular transport and fouling. In addition the theoretical chapter describes all characterization techniques ATR-FT-IR, XPS, streaming zeta potential and contact angle pH titration. Subsequently, the experimental chapter contains the synthesis procedure, execution of characterization and potential errors within the techniques. In the next chapter, results are presented and discussed with respect to the hypothesis. The thesis ends with a conclusion and recommendations for potential studies in the future.

2. THEORY

2.1 NANOFILTRATION MEMBRANES

Membrane performance is assessed in terms of permeance and retention. The permeance is the ability of a membrane to allow transportation of molecules or ions; often expressed as the material transported per unit area, time and driving force (flux) [mol m^2 s^{-1} Pa^{-1}]. The selectivity of a membrane is often depicted as retention (R) or separation factor (α) and depends on permeate to retentate concentration, see equation below. [3] A well performing and cost effective membrane offers both high flux and high selectivity. In addition, it should provide long-term mechanical stability, chemical and thermal stability under operating conditions as well as low fouling sensitivity. [2]

$$R = \left(1 - \frac{C_P}{C_R}\right) * 100\%$$

With
C_p: concentration of permeate
C_R: concentration of retentate

A membrane uses multiple kinds of driving forces for separation, for instance pressure, concentration gradients or electric potential differences or a combination of them. [2] Pressure driven membranes are classified as micro- ultra- and nanofiltration or reverse osmosis (RO). The pressure driven filtration methods differ in "pore sizes" and thus in particles or ions they sort. As the membrane density increases, the applied pressures to reach the same flux also increases. A schematic overview of pressure driven membranes is shown in Figure 1.

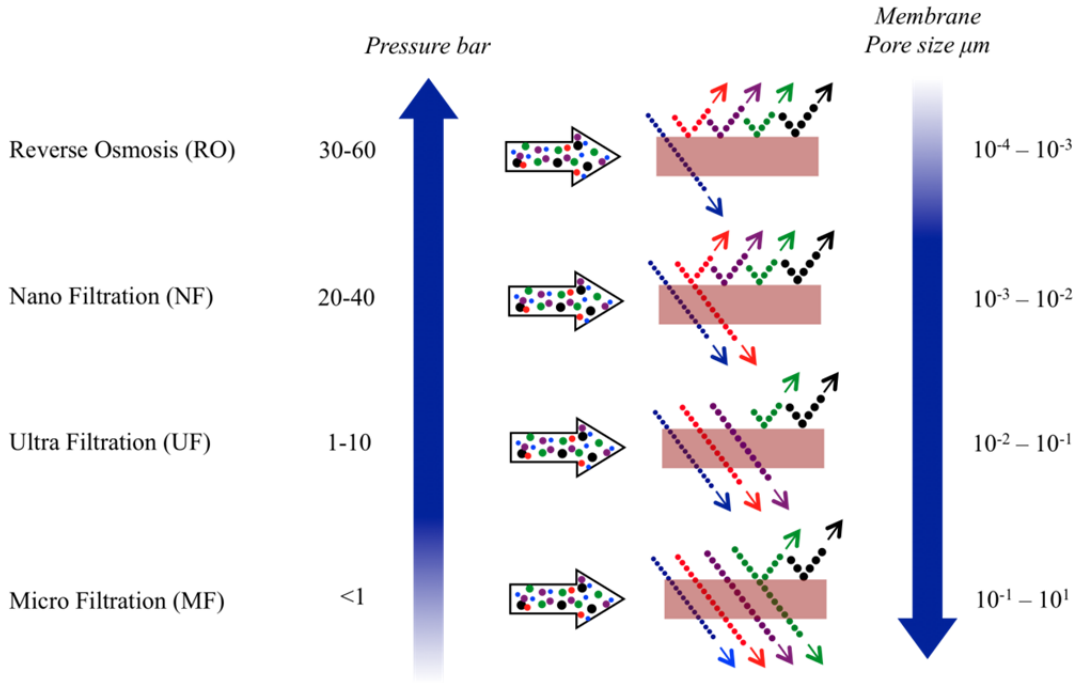

Figure 1: Schematic overview of membrane separation processes: reverse osmosis (RO), nanofiltration (NF), ultrafiltration (UF), microfiltraion (MF) and the corresponding properties such as pressure, separated ions and pore sizes. [12]

NF membranes provide both, a reasonable flux and good selectivity. NF is defined as open RO or tight ultrafiltration membranes with pore sizes of 5-10 nm. Usually water and monovalent ions permeate

through NF membranes. Multivalent ions and molecules from 200 to 1000 g/mol e.g. inorganic salts or glucose and sucrose can be separated off. [2] NF membranes completely dominate the market in water filtration. NF and RO membranes are particularly used for ocean, brackish water desalination and advanced water purification. [2] NF membranes allow lower operating pressures compared to RO and thus NF membranes are economically more efficient. [13]

2.1.1 Materials

Most RO and NF membranes are thin-film composite (TFC) polyamide membranes. TFC membranes compose a selective and a porous layer. Their excellent performance and superior economics is governed by individual layers that are tailored independently. [14] Most membranes consist of polymeric materials. Polymeric membranes show high flexibility in the design but suffer mainly from chemical instability. Polyamides are most commonly used for NF and RO. Benefits in the use of polyamides are high desalination rate, large flux, good chemical stability and low operating pressure conditions. [15] Dow Filmtec NF270 is nowadays the state-of-art membrane used for groundwater purification and soft drink production. The high active membrane area enables efficient removal of organic matter and the use of low operation pressures. Dow Filmtec NF270 membranes are composed of a piperazine-based polyamide layer on top of a microporous polysulfone support reinforced with a non-woven polyester backing layer. [16]

Fewer membranes are made of inorganic materials which own high chemical, thermal and mechanical stability compared to polymers. This is attributed to the stability of the bonds and the resistance to cleavage of covalent bonds in main or side chain. [2]

Dalwani et al [4] studied inorganic-organic hybrid membranes; comprising silica based (POSS) and carbon based precursors (multifunctional organic monomers). Research by Dalwani et al has shown that these hybrid membranes unite thermal-mechanical stability of inorganic materials with the versatility of organic polymers. The exceptional behavior is governed by homogeneous distribution of organic and inorganic moieties on a molecular level and a high degree of cross-linking. The hybrid characteristics of these networks allow advanced separation performance under conditions where polymer materials suffer from swelling or else. [4]

2.1.2 Interfacial Polymerization

IP pioneers the fabrication of TFC membranes, first performed by Thomas Cadotte [17]. Liquid-liquid IP promotes the reaction of two reactive species at the interface of immiscible liquids, of which one is preferably water and the other organic nature. IP involves a polycondensation reaction of an amine with a multifunctional acyl chloride. The reaction is effectively controlled by the interfacial area. Since the two phases are immiscible, the reaction solely takes place at the liquid-liquid interface forming a layer of about 100 nm thickness. An ultrathin layer is produced because the reaction is self-terminating. The membrane thickness is decreased by reducing diffusion rates, for instance, by poor solubility in the other solvent and short reaction times. [4, 18] Extensive studies on this fabrication technique and its kinetics are done by Cadotte [17] and for hybrid polyPOSS amide membranes by Dalwani et al [4]. The advantages of IP are the ability to potentially produce infinitely lateral macroscopic dimensions and the reaction at ambient temperature and pressure. In addition, IP enables the synthesis of ultrathin, homogeneous and defect-free films in the nanometer range (~100 nm). [4]

IP of TFC is performed on a porous support. The single steps taken in IP are shown in Figure 2. First, the porous support is wetted by a low-interfacial tension solution. Prewetting steps are often applied to stimulate the hydrophobic supports by increasing wettability with a surfactant solution.

Therefore, the penetration of aqueous amine solutions into pores is enhanced which facilitates a homogeneous polymerization reaction [4]. In the next step, aqueous amine solution amine can be flushed through the support until all pores are immersed. These flushing steps are often executed using slight underpressure to transverse the solutions through the substrate. After the immersion of the aqueous solution, the actual IP reaction is initiated by exposing the sample to the organic solution containing the multifunctional acyl chloride. The amines diffuse through the interface forming the films on the support. The product is a TFC membrane comprising an ultrathin polyamide layer on a porous support. [19]

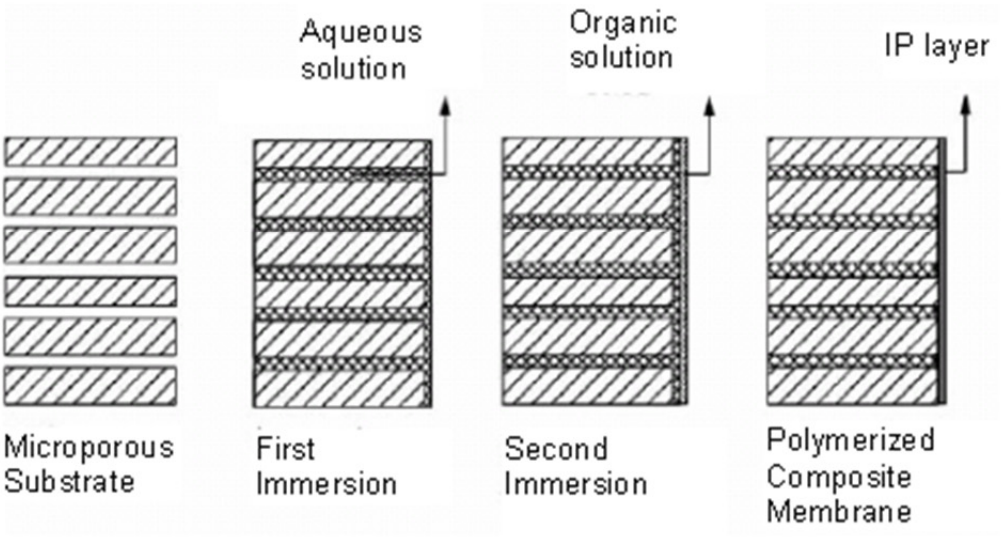

Figure 2: Schematic overview of TFC membrane synthesis steps via interfacial polymerization [18]

Reaction

IP of polyamides involves a polycondensation reaction, executed at ambient temperature which should avoid side reactions and thermal degradation. [4] The nucleophilic substitution reaction takes place between primary amines and acyl chlorides. There is a nucleophilic attack of the amine group to the carbon atom of the acyl chloride, forming an unstable intermediate. In the next step, the chloride atom leaves as it is a good leaving group and thus an amide bond is formed. The reaction mechanism is shown in Figure 3. The figure exemplifies the polycondensation reaction by the reaction of one functional group. A hyper cross-linked network can be synthesized if multifunctional monomers are used. The final product is then a covalently bonded polyamide network. An overview of the IP reaction of an octa-ammonium POSS and IDC is shown in appendix A, Figure 24.

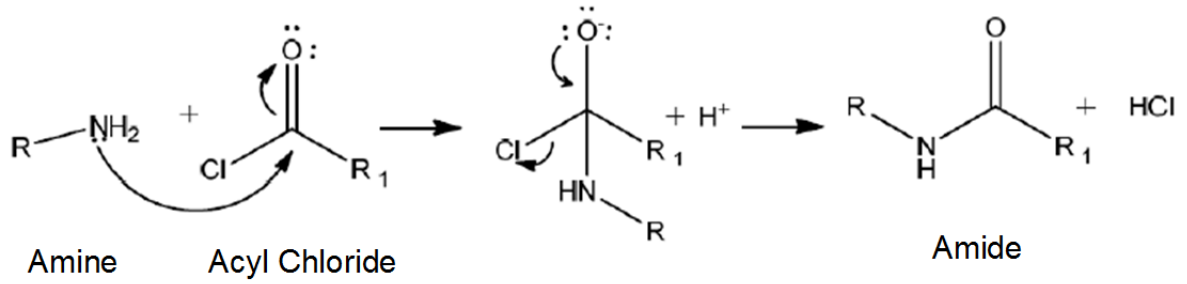

Figure 3: Reaction mechanism of an amide via condensation reaction. There is a nucleophilic attack of the amine group to the carbon atom of the acyl chloride, forming an unstable intermediate. Then, the chloride atom leaves as it is a good leaving group and thus an amide bond is formed. The figure exemplifies the polycondensation reaction by the reaction of one functional group. Since multiple functional groups exist, a hyper cross-linked network is synthesized. [20]

COMPONENTS

Octa-ammonium POSS was the inorganic amine source for the polycondensation reaction in this study. In particular, this work uses a water soluble octa-ammonium chloride salt functionalized POSS (POSS-$(CH_2)_3NH^{3+}Cl^-$); a three-dimensional structure assembled of 8 silsesquioxane units ($RSiO_{1.5}$), depicted in Figure 4. The cubic symmetry of the POSS cages enables a nanoscale 3D network formation. Additionally, the rigidness and bulky character of these cages strengthens networks. [4]

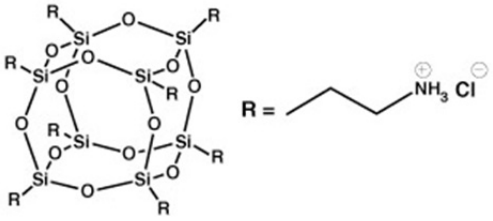

Figure 4: Chemical structure of octa-ammonium POSS [21]

The acyl chloride source for the IP reaction was IDC, see Figure 5. The choice of cross-linker is particularly important for the characteristics and thus application of the membranes. In previous studies trimesoylchloride (TMC) was used for nanofiltration applications, a trifunctional acyl chloride. IDC is expected to convert more acyl chloride groups to amide groups in the polycondensation reaction. This is rationalized by the difference in architecture since functional groups in IDC are less sterically hindered. As a result, less side reactions occur and IDC membranes should provide less negative charges on the membrane. [17], [22], [23] In addition, Mo et al [22] surmise that the use of IDC leads to improved anti-fouling properties with respect to calcium bridging to alginates compared to TMC. This is governed by expectations of less carboxylic acid groups present on IDC base membranes compared to TMC based membranes.

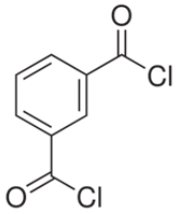

Figure 5: Chemical structure of isophthaloyl dichloride.

A porous PAN support is used in this study. This membrane is ascribed to ultra or microfiltration membranes. It has a smooth slightly negatively charged surface to accommodate defect free top layers.

INFLUENCE OF PH OF POSS SOLUTION

A general requirement to stimulate the polycondensation reaction of octa-ammonium POSS and IDC is an alkaline environment in the aqueous POSS solution [4]. Before the polymerization reaction can occur, octa-ammonium POSS has to be activated by alkaline solution to convert unreactive ammonia groups to reactive primary amine groups. A positive side-effect of alkaline POSS solution is the neutralization of HCl produced during the reaction. The alkaline condition needed is rationalized by the titration curve of octa-ammonium POSS obtained by Dalwani et al [4], shown in Figure 6.

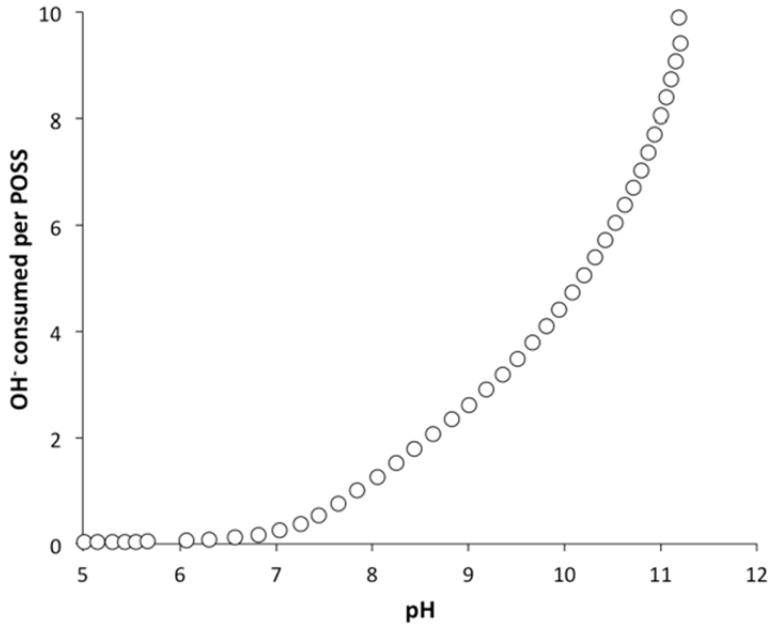

Figure 6: Amount of OH^- consumed per POSS cage as a function of pH of titration solution. [4]

The figure shows that the number of hydroxyl ions (OH^-) consumed per POSS cage increases logarithmically as a function of pH of the titration solution. The OH^- groups consumed are equivalent with the amount of amine groups present per POSS cage. Below pH 8 the activation of the POSS molecule is insufficient for IP since less than one reactive amine group is present. Conclusively, a minimum pH of the POSS solution of pH 8 is needed for the polycondensation reaction to occur. The upper limit of the pH of the POSS solution is pH 10; above pH 10 hydrolysis of POSS cages into ladder structures is dominant [4], shown in Figure 7. This would result in a less homogeneous and less stable network. It might also be possible that at high pH acyl chloride groups of IDC molecules are converted to carboxylic acid groups [17] which in turn would lead to hamper IP so that no network would be synthesized.

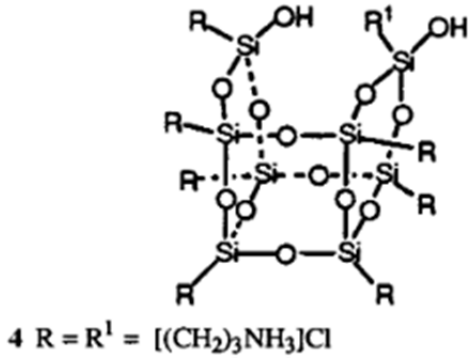

Figure 7: Ladder structure of octa-ammonium POSS cage. [24]

2.1.3 Transport Mechanisms

NF techniques separate based on size exclusion and membrane-solute interactions. Particularly important for NF separation performance are external and internal electrostatic interactions between ions in mixtures and membrane surface charges. This principle is supported by the fact that

NF membrane pore diameter (1< d_p <4 nm) are much larger than the hydrated ion diameters (d_{ion}^{h}= 0.4 nm). [5]

Molecular transport of components through non-porous and porous selective layers, are expressed in terms of the solution-diffusion model and the pore-flow model, respectively. [25] The choice of the model depends on the porosity of the membrane. A porous material possesses free volume elements which are relatively large and constant in terms of position and size. A non-porous material owns pore sizes < 5 Å which are variable due to thermal motion of polymer chains. Although NF membranes are on the cutting edge to RO and ultrafiltration membranes; solution- diffusion models are often applicable since NF membranes are considered to be dense. [13] This model deals with two mechanisms sorption and diffusion of the species. It presumes that ions are dissolved in the membrane-water interface; then they diffuse through it and finally they desorb again. Therefore, separation in NF is dominated by Donnan-exclusion effects (charge-effect) [13], [26], [5], meaning same charges are soluble and oppositely charged ions will be repelled by the membrane surface. [2] An illustration of this principle is shown in Figure 8.

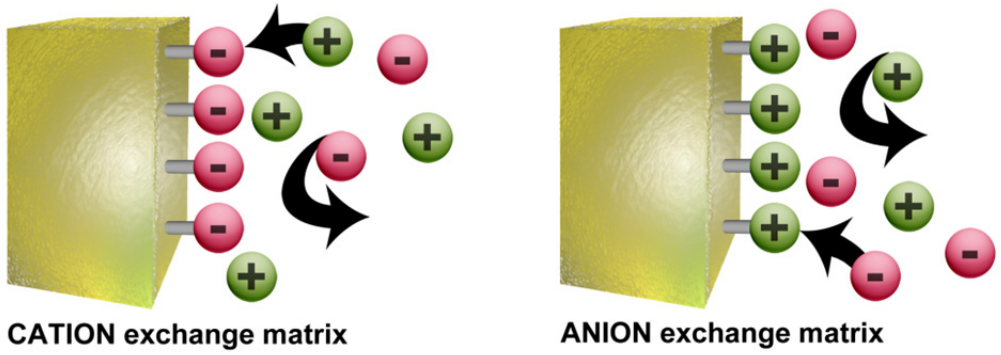

Figure 8: Schematic of the Donnan-exclusion effect for positively charged membranes (anion exchange matrix) and negatively charged membranes (cation exchange matrix) [27].

In most cases, membranes are negatively charged. Polymeric membranes often have unreacted moieties which is governed by steric hindrance that prevent the reaction. If the unreacted moieties come in contact with water, membranes acquire surface charges due to dissociation of surface ionic groups, usually of acidic nature. Therefore, negatively charged membranes reject anions in solutions with low pH values. [28] The dissociation of charged groups also affects the “openness”. If membranes possess dissociable groups, they demonstrate a more open structure in basic environment, potentially influencing the separation by size exclusion. [29]

There is also the possibility of an ampholytic behavior of the membranes. Ampholytic membranes repel positive and negative charges due to basic and acidic groups attached to the membrane surface, respectively. [28] If the solute is neutral, membrane rejection only increases in proportion to solute size (e.g. lactose, sucrose). [2]

Another theory for transport across charged membrane is the dielectric exclusion principle. There the water is polarized in the pores by the charge of the membrane. The polarization results in a decrease of the dielectric constant inside the pore which in turn limits the entering ability of charged solutes to the pores. On the other hand, if ions are transferred to the pores the electrostatic free energy changes. This also leads to exclusion. However, in NF most literature focuses on the Donnan-exclusion as the major distribution mechanisms. [30]

2.1.4 Charge Effect on Fouling

Chemical and charge character drastically affect the NF membrane performance since pore sizes are in the nanometer range. For instance, membrane hydrophilicity and also tendency to fouling are strongly influenced by the charge nature of the membrane. [31] Especially fouling is a main issue of research in membranes technologies. Fouling is induced by particles in the feed, often organic in nature, which deposit on the membrane surface and are not removable by periodic cleaning. This inhibits trans-membrane permeability and decreases the life time, which finally results in an increase in maintenance and operating costs of the process. Therefore, it is desirable to prevent fouling from the beginning.

Fouling is expected to originate from binding affinity of membrane surface and fouling agent. The hydrophilicity and electrical charge of membranes are surmised to influence membrane fouling properties. [32, 33] Adsorption of foulants occurs mainly via charge, dipole-dipole, hydrogen bonding and van-der-Waals interactions. Hydrophilic membranes are less sensitive to organic fouling. This is due to the dipole-dipole interactions of water and membrane surfaces. Therefore, a water layer is attached to the membrane surface that inhibits to bind organic fouling. Positive and negative charges on membrane surfaces increase the hydrophilicity of membranes.

2.2 Characterization

2.2.1 Attenuated Total Reflection - Fourier Transform - Infrared Spectroscopy

Infrared spectroscopy (IR) identifies functional groups present in a compound. It measures the absorption of infrared light on matter. IR light causes vibrational excitation of the molecule. There are two modes of vibration of the functional groups; bending which is assigned to a change in bond angle and symmetric or asymmetric stretching relating to a change in bond length. In an IR spectrum, the intensity is represented as a function of wavenumber (cm^{-1}) which is proportional to frequency. The IR spectrum is divided in two regions: the fingerprint region which is unique for every molecule (0-1500 cm^{-1}) and the diagnostic region (> 1500 cm^{-1}). The wavenumber is affected by mass and bond strength – smaller atoms and stronger bonds vibrate at higher frequencies. The number of resonance structures defines the strength of a bond; the more resonance structures one molecule possesses, the more stable the bonds. The intensity is influenced by the number of bonds that cause the signal and by the strength of the dipole moment of the functional group. IR absorption is caused by dipole moments and thus the stronger the dipole moment, the more intense the peak. The shape refers to different stages of hydrogen bonding. Hydrogen bonding shifts the peak location which causes the broadening of a certain peak. Nevertheless, not everywhere the hydrogen bonding is strong enough to shift the peak location. Fourier transformation is the calculative approach to obtain absorption spectra, resulting in an interferogram. [34]

ATR-FT-IR enables to identify functional groups of thin films. The penetration depth is typically below 1 µm. [14] The key difference in ATR-FT-IR is that it measures the intensity loss after multiple reflections, wherefrom it generates the absorption spectrum. A schematic view of the working principle is shown in Figure 9.

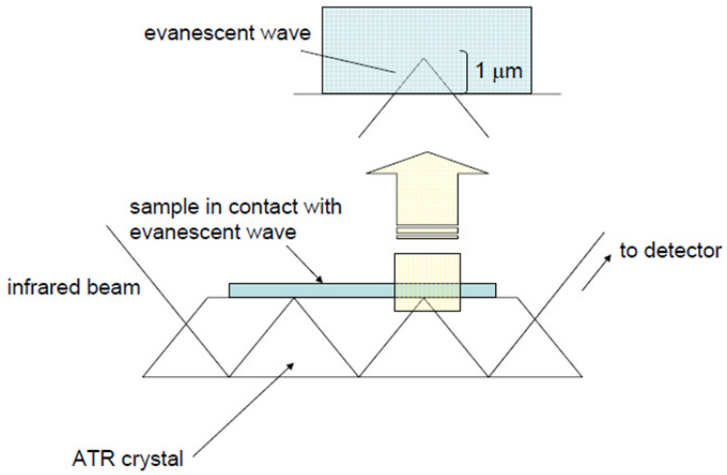

Figure 9: Schematic view of attenuated total reflection infrared spectroscopy. The incoming IR beam is multiple times reflected between sample surface and ATR crystal before it is detected and an interferrogram is obtained. [35]

2.2.2 X-RAY PHOTOELECTRON SPECTROSCOPY

XPS is a spectroscopic technique to investigate the surface properties from 0.5 nm to 10 nm depth. It identifies stoichiometry and chemical state of surface elements by analysis of the binding energy. The sample is exposed under ultra-high vacuum to mono-energetic x-rays which excite electrons of the surface atoms. If the binding energy is lower than the x-ray energy (*hv*), the excitation results in emission of photoelectrons. This principle is illustrated in Figure 10. From the kinetic energy and scattering of photons, the binding energy and intensity is determined. An XPS spectrum depicts the emission intensity versus the binding energy. Hereby information about elemental identity, chemical state and quantity of an element can be deduced [36],[37]. Core binding energies in eV are determined by electrostatic interactions between nucleus and electrons and are unique for each element. [2] Chemical shifts in binding energies are introduced by the electrochemical environment. The withdrawal of valence electrons increases binding energies and the addition of valence electrons decreases binding energies. The intensity of the photoelectron peak for a certain element is proportional to the average atomic concentration in the analysis sample, the photoelectron cross-section of the element and the free mean path. [38]

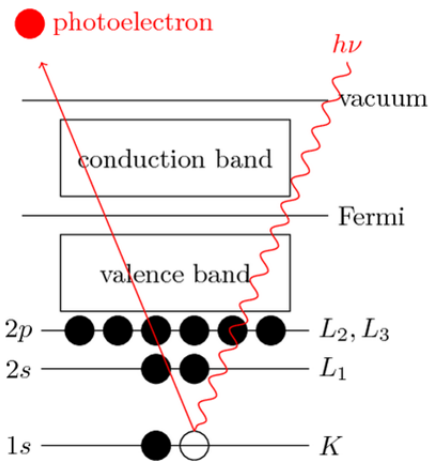

Figure 10: Principle of X-ray photoelectron spectroscopy. The X-ray energy (*hν*) excites and emits a photoelectron with a certain kinetic energy. K, l_i and 1s,2s, 2p label the shells or orbital, respectively. [39]

2.2.3 ZETA-POTENTIAL

The determination of surface charge is crucial for understanding membrane separation performances as well as surface fouling phenomena. Streaming potentials are often used to investigate the zeta potential of membranes and thus the interfacial and colloidal behavior. Zeta potential (*ζ*) is a measure of ionization of a non-neutral surface. It is also named electrokinetic potential and located in the electric double layer (EDL) of a surface. A schematic view of the electric double layer is shown in Figure 11. By way of example, unreacted chlorines of acyl chlorides in water will form carboxylic acid. In a certain pH environment this group will be depronated, leading to immobile negative charges on the membrane. The aqueous phase tries to balance the negatively charged surface and thus positive counter charges are posed onto the surface. This configuration is known as EDL. The EDL composes an inner region (i.e., Stern layer) where counter ions to the surface charges are strongly bound and immobile. In the outer diffusion region, ions are loosely bound and more mobile. The outer diffusion region, takes thermal motion of ions into account and thus a Boltzmann distribution is assumed. Therefore, electrostatic interactions near the solid surface as well as the charge density decreases to that of the bulk. The zeta potential is the potential difference in between the dispersion medium and the stationary layer (i.e., shear plane) of the fluid on a solid surface, shown in Figure 11. [40]

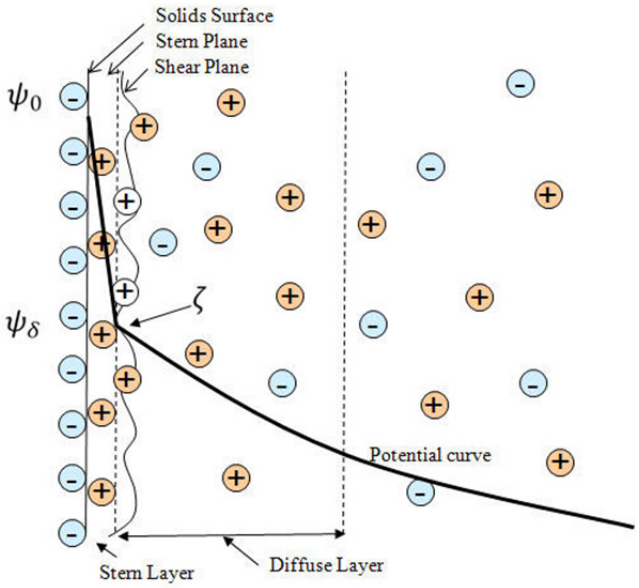

Figure 11: Schematic of the electric double layer on membrane surface according to stern model consisting of an immobile stern layer and a diffusion region. [41]

The isoelectric point (IEP) defines the point of no net electrical charge. The net charge is affected by the pH surrounding environment in which the solid is submerged. [40] The IEP is calculated by the average of the acidity constants (pKa_i) of the component present, see formula below. This formula is only valid if one type of positive and negative groups is present, respectively. [42]

$$IEP = \frac{pKa_1 + pKa_2}{2}$$

Streaming Zeta Potential

Zeta potential (ζ) is a useful characteristic for investigating the EDL since the surface potential cannot be measured directly. Streaming zeta potential measurements are used to determine the surface charge of a membrane over a range of pH values. This technique uses a pressure induced flow of an electrolyte solution through channel geometry covered with membrane samples. A hydrodynamic flow is introduced by a pressure difference and ions from the diffusive layer are forwarded which leads to a streaming current. The zeta potential for solid materials with planar surface is calculated by the Helmholtz and Smoluchowski (HS) approach, shown in equation below. Thereby, the change in streaming potential *dU/dp* is measured per change in pressure and related to the cell constant *L/A* of the streaming channel. Note that measuring the potential instead of current increases the error because also the resistance has to be measured. This resistance can also be influenced by cell edge conductivity which enlarges the error in measurement. The gap height is calculated from the volume flow rate measured and the generated differential pressure. [43]

$$\zeta = \frac{dU_s}{dP}\frac{\eta}{\varepsilon\varepsilon_0}\frac{L}{A}\frac{1}{R}$$

With,

dU_s: change in streaming potential

dP: change in pressure

η: electrolyte viscosity

ε: dielectric constant of the electrolyte

ε_0: vacuum permittivity
L: cell length
A: cross-sectional area
R: cell resistance

CONTACT ANGLE PH TITRATION

Contact angle titration is another approach to identify the zeta potential. In theory, the surface charge density and thus zeta potential can be investigated by contact angle titration with unbuffered solutions as shown by Hurwitz [44] and Rosa [45]. In this case, the solution is buffered by the surface functional groups. The breakpoint of the unbuffered titration curves is reached when the buffering of ionizable functional groups at the membrane surface fails. Thus, the number of e.g. hydroxide ions equals the total number of acidic functional groups at the surface; corresponding to the maximum charge density of the membrane. The breakpoint is reached when the slope of the curve first deviates from zero. [44]

Another aspect derived from contact angles is the wettability of surfaces. By definition, a contact angles larger than 90° characterize hydrophobic surfaces. Contact angles smaller than 90° indicate a hydrophilic nature of surfaces and thus better wettability. An overview of hydrophilic and hydrophobic surfaces with corresponding characterisitcs of contact angle, adhesiveness and wettability is shown in Figure **12**.

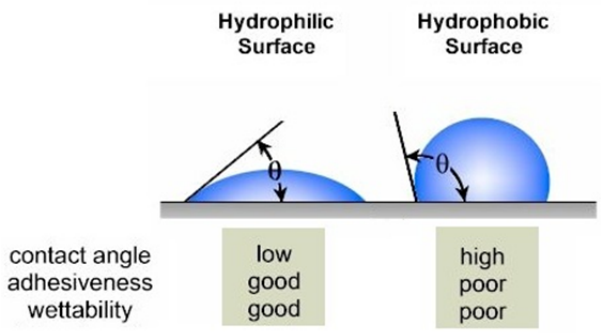

Figure 12: Overview of hydrophilic and hydrophobic surfaces with corresponding characteristics of contact angle, adhesiveness and wettability.[46]

3. EXPERIMENTAL

3.1 CHEMICALS

Chemicals used, were supplied by Sigma Aldrich: 1,3-Benzenetricarbonyl dichloride (Isophthaloyl Dichloride, 98 %), Hexane (anhydrous, 99.8 %) and dodecyl sulfate sodium salt (SDS, >99%). Octa-ammonium POSS® was purchased at hybrid plastics. Q2 Millipore water was used to make aqueous solutions. A nonwoven polyacrylonytrile (PAN) support was purchased from SolSep. All chemicals were used as received.

3.2 MEMBRANE SYNTHESIS

Five membranes of octa-ammonium POSS and IDC (cross-linker) were synthesized by IP. The POSS solutions were prepared at different pH values: pH 8.3, 8.7, 9.1, 9.5, 9.9. The range from pH 8-10 is most appropriate for promoting the IP reaction and preventing a large amount of cleaved POSS cages. Octa-ammonium POSS (0,9 wt%) was first dissolved in water and activated by adjusting the pH value with sodium hydroxide (1 M) to either of the pHs mentioned above. Next, 0.075 wt% IDC was dissolved in n-hexane for the organic phase. IP was performed on an ultra-porous, nonwoven PAN support membrane. The support was glued with double sided tape on a metal module with vacuum connection**.** It is important to glue the supportive materials thoroughly on the sample holder to prevent leaking in the impregnation steps. Then the membrane was prewetted for 15 minutes at slight under-pressure (0.5 bar) using a SDS solution (0.05 wt%). The negatively charged surfactant (SDS) improves wettability of the PAN support and thus the occurrence of the IP reaction. In the same manner as the prewetting step, the aqueous POSS solution impregnated the PAN support for 15 minutes. After this step, the membrane was dried for approximately 15 minutes until no solution was left on the support surface. The polymerization reaction was performed by exposing the membrane-module to the IDC/ hexane solution for a reaction time of 5 minutes. After the reaction, the membrane-module was rinsed with acetone to remove residuals of hexane. A general advice is to keep all non-varied synthesis parameters constant such as reaction time and concentrations of solutions.

3.3 MEMBRANE CHARACTERIZATION

3.3.1 ATTENUATED TOTAL REFLECTANCE- FOURIER TRANSFORM- INFRARED SPECTROSCOPY

ATR-FT-IR was performed using an ALPHA FT-IR Spectrometer (Bruker Optics Inc, Germany) equipped with a ZnSe crystal. A background measurement was executed to exclude influences from air or else. Dry and clean membrane samples were placed on the crystal and measured at room temperature. Uncertainties of intensities in the spectra with an absolute shift can result from differences in contact between crystal and sample or thickness of the membrane film. Spectra were normalized with respect to a certain peak to make different spectra comparable.

3.3.2 X-RAY PHOTOELECTRON SPECTROSCOPY

XPS was performed on a Quanteria SXM scanning XPS microprobe (Physical Electrons) using a monochromatic Al Kalpha source (1486.6 eV) under ultra-high vacuum. The spectra provided by the XPS equipment were analyzed using peak analyzer in origin. The error estimations were based on standard error in estimations of peak analysis. Chemical shifts in XPS spectra of max. 0.2 eV were

assigned to the use of different XPS analysis equipments. Deviations from expected binding energies were expected to be mainly caused by contaminations of the membrane surface.

3.3.3 Streaming Zeta Potential

The streaming zeta potential pH titration was analyzed using a SurPASS Electrokinetic Analyzer (Anton-Paar, Graz, Austria) with the adjustable gap cell. Two samples of one membrane of 20 mm x 10 mm were glued with double sided tape on the sample holders of the gap cell. An electrolyte solution of 5 mM KCl was titrated over a pH range from pH 4-10. It is important to use the same electrolyte concentrations for every membrane to make different zeta potential measurements comparable. Three rinsing steps with each 800 s followed with demi-water, 5 mM KCl and 5 mM KCl adjusted to pH 4, respectively. While rinsing, the gap height was adjusted to ~140 µm. During the measurement, pH value of the electrolyte solution was adjusted using 0.1 M nitric acid (HNO_3) and 0.1 M sodium hydroxide (NaOH), respectively. After rinsing, a flow check was executed to ensure the same flow properties in forward and backward flow. In the measurement, four points for each pH values were measured - two per flow direction to reduce possible errors. The evaluation of zeta potential was calculated by the Helmholtz and Smoluchowski (HS) approach which is usable for planar geometries.

3.3.4 Contact Angle pH Titration

Contact angle titration was performed on OCA 15 Dataphysics, Germany. Sessile drop equilibrium contact angle measurements were executed on the membrane surfaces. Aqueous solutions were adjusted to pH values ranging from pH 4-10 by 10 mM HCl and 10 mM NaOH solutions, respectively. Unbuffered aqueous titration solutions of pH 4, 5.5, 7, 8, 9, 10 were used. Droplets 1µl in volume were exposed to the membrane surface and measured five seconds after placing on the membrane surface. Contact angles were measured between the baseline of the droplet and the tangent of the liquid-air interface. It was crucial to measure at fixed times since the IDC POSS membranes are water permeable and droplets will eventually be soaked into the membrane. As observed from trial measurements, faster changes would occur after 15 s. Conclusively, 5 s measurements would merely result in small deviations if the measuring time varies. Five droplets were measured per titration solution and membrane to minimize the errors by averaging. Physical and chemical properties of the membranes strongly influence the measured contact angles and might be misleading in deductions. [29]

4. RESULTS & DISCUSSION

4.1 SYNTHESIS

Table 1 shows the IDC POSS membranes synthesized. The table displays the synthesis pH, date, characterization method executed and concentrations of solutions used in interfacial polymerization for each membrane. It should be mentioned that two different samples of the membranes synthesized at pH 9.1, 9.5, 9.9 are used in the characterization as shown in the table. However, as all samples were produced under same conditions, it is assumed that they should provide the same trends.

Table 1: Synthesized IDC POSS membranes with corresponding characteristics such as synthesis pH, date of synthesis, characterization method employed and concentrations of solutions used in the reaction.

Synthesis pH of Membrane	Date of Synthesis	Characterization	Inorganic Monomer	Organic Monomer	SDS solution
8.3	16/4/2014	IR, XPS, Zeta	0.9 wt% octa-ammonium POSS/ water	0.075 wt% IDC/ Hexane	0.05 wt% SDS/ water
8.7	23/4/2014	IR, XPS, Zeta			
9.1	16/4/2014	IR, Zeta			
	20/3/2014	XPS			
9.5	21/4/2014	IR, Zeta			
	7/3/2014	XPS			
9.9	23/4/2014	IR, Zeta			
	17/3/2014	XPS			

4.2 CHARACTERIZATION

The chemical nature of the membranes with respect to component analysis, polymerization state and hydrolysis of POSS cages was deduced from ATR-FT-IR and XPS spectra. In addition, XPS provided information about surface properties such as stoichiometry of elements and oxidation states of functional groups. Therefore, most importantly, amine, amide and positively charged ammonia groups were distinguishable. Streaming zeta potentials measurements were performed to obtain zeta potentials which characterize surface charges. Contact angle pH-titration failed to give insight in surface charges but provided information on hydrophilicity of membranes.

4.2.1 ATTENUATED TOTAL REFLECTANCE INFRARED SPECTROSCOPY

The chemical of structure polyPOSS amide membranes was determined by ATR-FT-IR. The functional groups expected were analyzed and stretching vibrations were gathered from Socrates, 2001 [47]. The peak analysis is depicted in Appendix B, Table 2. The IR absorbance spectra of the PAN support (bottom line), octa-ammonium POSS (middle line) and IDC POSS film synthesized at pH 8.3 (top line) are shown in Figure 13. The PAN and octa-ammonium POSS spectra serve as a reference. The presence of POSS cages in the IDC POSS samples is confirmed with peaks at 1040 cm^{-1} and 1125 cm^{-1}. The two stretches represent the ladder and polyhedral structure of the POSS cages, respectively.

Further, the existence of the IDC phenyl rings in the membrane samples is indicated with peaks 1506 cm^{-1}, 1614 cm^{-1} and 3068 cm^{-1}, 3032 cm^{-1}. The peaks are associated with conjugated carbon bonds in the phenyl ring (C-C) and stretching vibrations for the carbon hydrogen stretch (C-H) of the phenyl ring, respectively. Noteworthy is that the stretches identified for the phenyl ring just

adumbrate the presence of phenyl rings since they are overlapping with stretches of the octa-ammonium POSS spectra. The validation for the presence and bridging function of organic moieties in polyPOSS amide membranes is shown in subsequent analyses.

The stretching vibration at 2240 cm-1 in the IDC POSS spectrum is originating from the PAN support of the nitrile group (C≡N) of the PAN support. This suggests that the synthesized film is indeed smaller than 1 µm as expected.

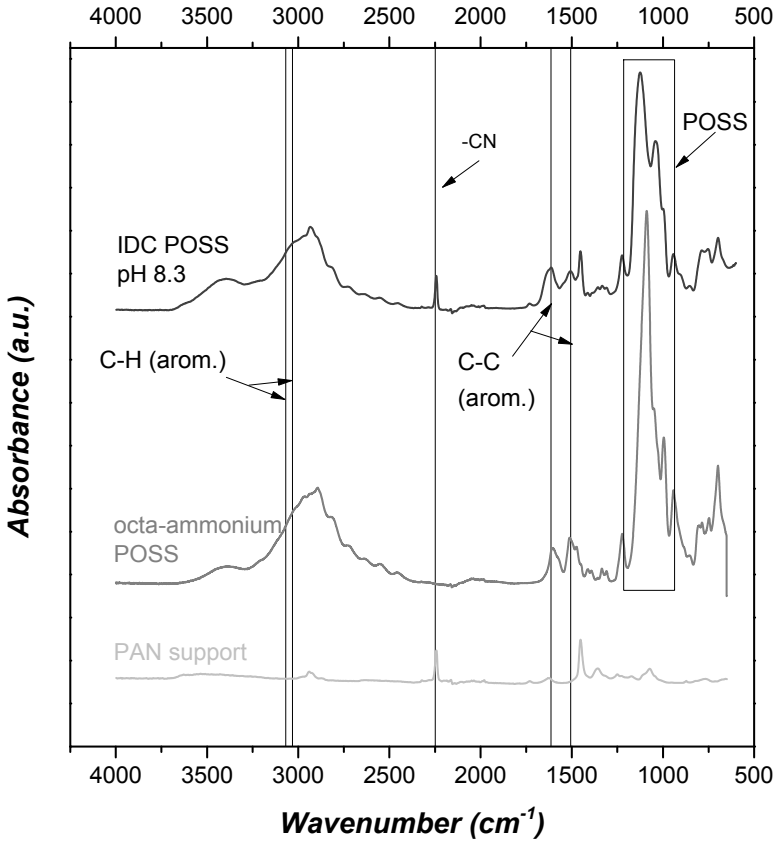

Figure 13: IR absorbance spectra of the PAN support (–), octa-ammonium POSS (–) and IDC POSS at pH 8.3 (–) as a function of wavenumber. POSS cages are identified by 1040 cm^{-1} and 1125 cm^{-1} stretches, representing the ladder and polyhedral POSS cage structures, respectively. The phenyl ring of IDC shows characteristic vibrations at 1506 cm^{-1} and 1614 cm^{-1} for the conjugated carbon bond in the aromatic ring (C-C) and 3068 cm^{-1} and 3032 cm^{-1} for the carbon-hydrogen stretch in the ring. The PAN support is responsible for the stretch at 2240 cm^{-1} which originates from the nitrile group (C≡N).

The ATR-FTIR spectrum close-up from 1800-600 cm^{-1}, shown in Figure 14, validates that POSS cages are incorporated in the hybrid polymer network. The ATR-FTIR spectra are given as normalized absorbance as a function of wavenumber in cm^{-1}. The absorbance spectra for each membrane synthesized at a different pH (colored differently) were normalized with respect to the polyhedral POSS peak at 1125 cm^{-1} for comparability. The existence of a hybrid polymer network is proofed with the occurrence of peaks characteristic for amide bonds. The comparison of the polyPOSS amide spectra show the attributed peaks for amide bonds at 1550 cm^{-1} (N-H stretch), 1640 cm^{-1} (C=O stretch) and 1200 cm^{-1} (C-N stretch) are progressively emerging when reaching higher synthesis pH values. The amide groups connect the POSS cages and organic bridges. The emerging of the peaks is explained by the fact that more ammonia groups of POSS cages are converted to primary amine groups. The primary amine groups participate in the polycondensation reaction and thus more amide

groups give the intensity rise in the spectra. At low synthesis pH values, it is hard to distinguish the amide peaks and thus, the presence of network is not conclusive any longer. The macroscopic integrity of POSS cages influences molecular selectivity in liquid permeation and thus was investigated further.

The fact that POSS cages are progressively hydrolyzed with increasing pH values is also seen in Figure 14 and supported by XPS analysis of Si2p peaks shown in Appendix C, Figure 26. The polyhedral and ladder structure of the siloxane group (Si-O-Si) have characteristic asymmetric stretching vibrations at 1125 cm^{-1} and 1040 cm^{-1}, respectively. Figure 14 clearly shows that the peak which refers to the ladder structure increases in intensity as the synthesis pH of the membrane increases. Conclusively, there is an increasing amount of ladder structures for higher synthesis pHs which confirms the expectations. Cleavage of POSS cages results from a high concentration of hydroxyl ions (OH^-), which attach to the silicon corners and break up the cages structures and result in ladder structures of the POSS (see Figure 7).

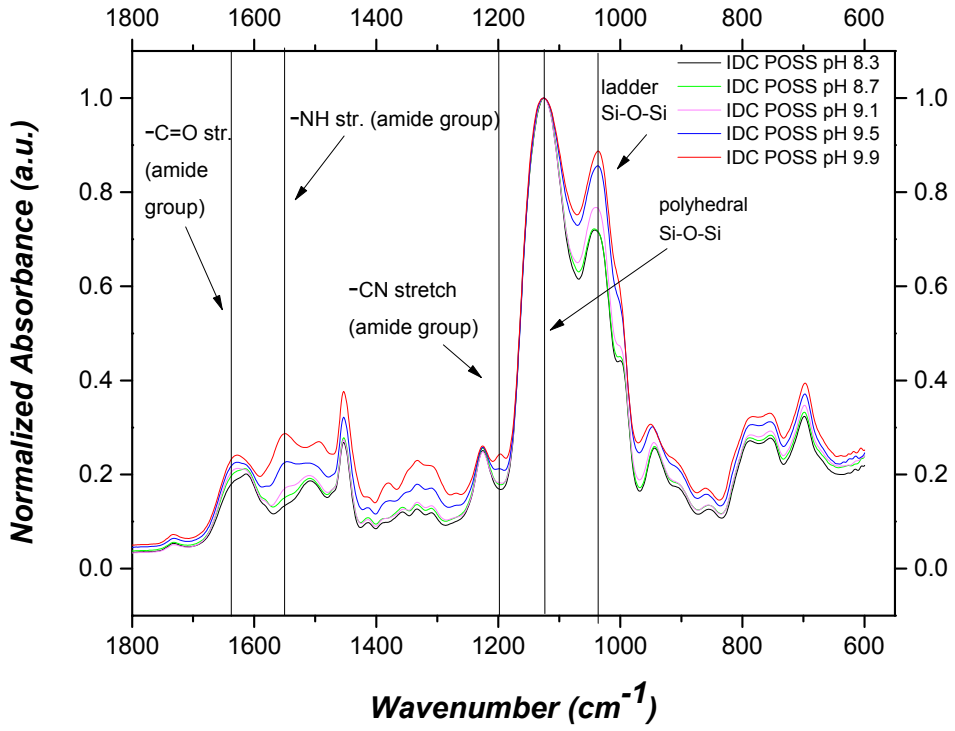

Figure 14: Normalized IR absorbance spectra of IDC POSS prepared at various pH values (pH 8.3 –, 8.7 –, 9.1 –, 9.5 –, 9.9 –). The absorbance was normalized with respect to the polyhedral POSS peak at 1125 cm^{-1}. Peaks at 1040 cm^{-1} and 1125 cm^{-1} are associated with the ladder and polyhedral structures of the POSS cages. Stretching vibrations at 1550 cm^{-1}, 1640 cm^{-1} and 1200 cm^{-1} belong to the amide groups ascribed to N-H stretch, C=O stretch and C-N stretch, respectively.

The degree of hydrolysis of POSS cages as a function of synthesis pH of IDC POSS membranes is shown in Figure 15. It was calculated by intensity ratios of the ladder and polyhedral POSS peaks. The graph shows that the hydrolysis percentage of POSS cages increases as the synthesis pH of the membrane increases. It shows that at pH 8.3, roughly 42 % of POSS cages have been hydrolyzed and at pH 9.9 ~47 %. The influence on molecular selectivity and or flux has to be investigated by permeation experiments. In any case, the percentages of hydrolysis of POSS cages give just an indication and cannot be taken as absolute. This is due to the fact that IR is not reliable with respect to intensity.

Stretching vibrations attributed to ammonia groups are overlapping with aliphatic carbon and amide vibrations in the second part of the spectrum 3800 cm^{-1}- 2200 cm^{-1}, shown in Appendix B, Figure 25. The examination of positive charges is done by XPS data analysis since no qualitative data can be obtained from the second part of the IR spectrum.

In brief, the ATR-FT-IR analysis shows that POSS cages are covalently linked by aromatic amide bridges to organic moieties and thus a polyPOSS amide network was synthesized. In addition IR deductions validate part of the hypothesis. In particular, IR data suggests that the higher the pH value in the synthesis, the larger is the degree of cross-linking but concomitantly the hydrolysis of the POSS cages increases.

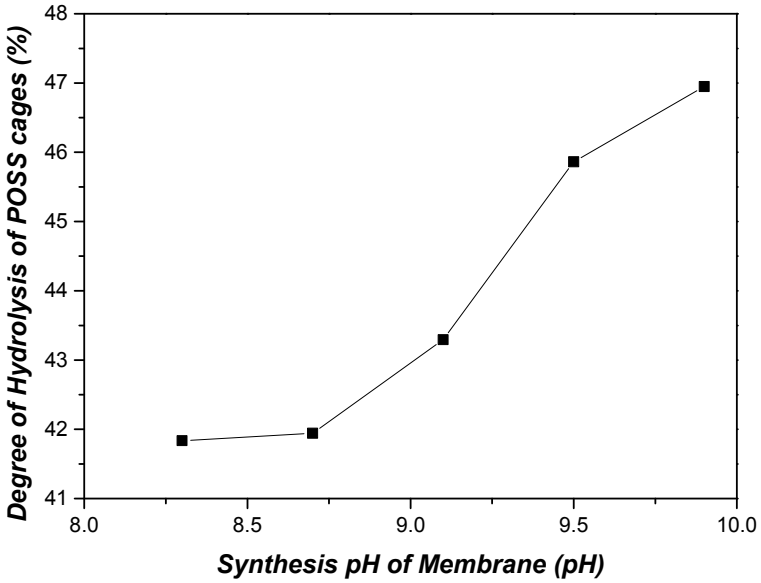

Figure 15: Degree of hydrolysis of POSS cages as a function of synthesis ph of IDC POSS membranes. The degree of hydrolysis was calculated by intensity ratios of the ladder and polyhedral POSS peaks.

4.2.2 X-RAY PHOTOELECTRON SPECTROSCOPY

The XPS results provide a diversity of information about the membranes. The subsequent analysis focuses on the stoichiometry, charges on the membrane and the degree of cross linking. Especially, the carbon and nitrogen high resolution scans were investigated. Results clearly confirm a trend of accumulation of positive charges with decreasing synthesis pH of the polyPOSS amide membranes. In addition, it shows that IDC is a cross-linker with high polymerization ability and thus a low amount of carboxylic acid groups are present on each membrane. The analysis of binding energies of octa-ammonium POSS and IDC peaks is shown in Appendix C, Table 4. In evaluation of peak fits, the analysis of small percentages of peak areas in the spectra have to be handled with care since base line corrections are an estimation and signal-to-noise ratios often decrease.

STOICHIOMETRY

Elemental concentrations of octa-ammonium POSS (theoretical values) and IDC POSS membranes synthesized at different pH values are shown Figure 16 and in Appendix C, Table 3. The oxygen (O1s –), nitrogen (N1s –), carbon (C1s –), chloride (Cl2p –) and silicon concentration (Si2p –) are given for

every IDC POSS membrane and octa-ammonium POSS as comparison. The elemental concentrations of carbon show an increase about 20 % compared to carbon concentrations of octa-ammonium POSS. The carbon concentration of the polyPOSS-amides is raised by the implementation of the organic phenyl bridges from the IDC molecules. A variety in elemental concentrations of the different polyPOSS-amide membranes complicates the deduction of trends in the concentrations. For that reason, subsequent analyses were executed.

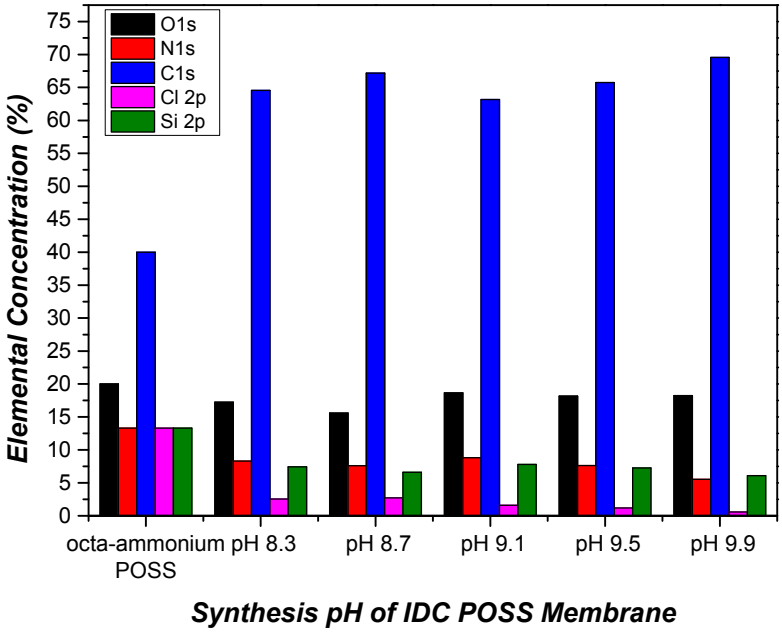

Figure 16: Elemental concentrations of octa-ammonium POSS and IDC POSS membranes synthesized at various pH values (pH 8.3, 8.7, 9.1, 9.5, 9.9). Different bars depict the oxygen (O1s –), nitrogen (N1s –), carbon (C1s –), chloride (Cl2p –) and silicon concentration (Si2p –).

Positive Charges on Membranes

The positive charges on the membrane are higher for polyPOSS-amides prepared with lower pH values, shown in Figure 17. The figure shows a comparison of the polyPOSS-amide high resolution scans of N1s for each membrane prepared at different pHs and a reference spectra of octa-ammonium POSS. Every spectrum is depicted as the intensity versus the binding energy in eV. The scan of the N1s peaks of octa-ammonium POSS (top) shows two peaks at 398.8 eV and 400.9 eV attributed to partially deprotonated ammonia groups (NH_2) and ammonia groups (NH_3^+), respectively. When comparing the polyPOSS-amide and octa-ammonium POSS XPS spectra, a chemical shift of ~0.2 eV is observed. The chemical shift is ascribed to different measurement equipments used for polyPOSS amides and octa-ammonium POSS.

The polyPOSS amide spectra show next to the primary amine and ammonia peak, a third strong peak around 399.77 eV, identifying the amide group (NCO). In agreement with the IR spectra, the amide peak confirms that a cross-linked film was synthesized also for membranes prepared with low pH solution. Chemical shifts within the polyPOSS-amide membranes might originate from the amount of counter ions present (Cl^- or OH^-). There is a high chemical shift ~0.5 eV in the membrane prepared at pH 8.7 which might have multiple reasons such as contaminations or mistakes in preparation procedure. It might also arise from the facts that in this membrane more acidic groups are present where more valence electrons would be withdrawn. It is advisable to synthesize and characterize the membrane prepared at pH 8.7 again.

Most importantly, the comparison of the spectra in Figure 17, show the ammonia peak emerging around 401 eV in the polyPOSS amide spectra when reaching lower synthesis pHs. This indicates an accumulation of positive charges for lower synthesis pHs and confirms the hypothesis. There is a total chemical shift of 0.5 eV within polyPOSS amide spectra which is most likely caused by the counter ions present in each membrane.

In addition, the comparison of spectra shows solely small peaks at 398.8 eV. This confirms anticipations, as the NH_2 groups are expected to have only minor contribution in the polyPOSS amide spectra. Most of the reactive amine groups have participated in the polycondensation reaction. It might also be that there is no amine group present since the baseline settings are estimates and signal-to-noise ratios are smaller than 3. As the signal-to-noise ratio is larger than 3, detection limits are acceptable; meaning that signals can be considered as peaks.

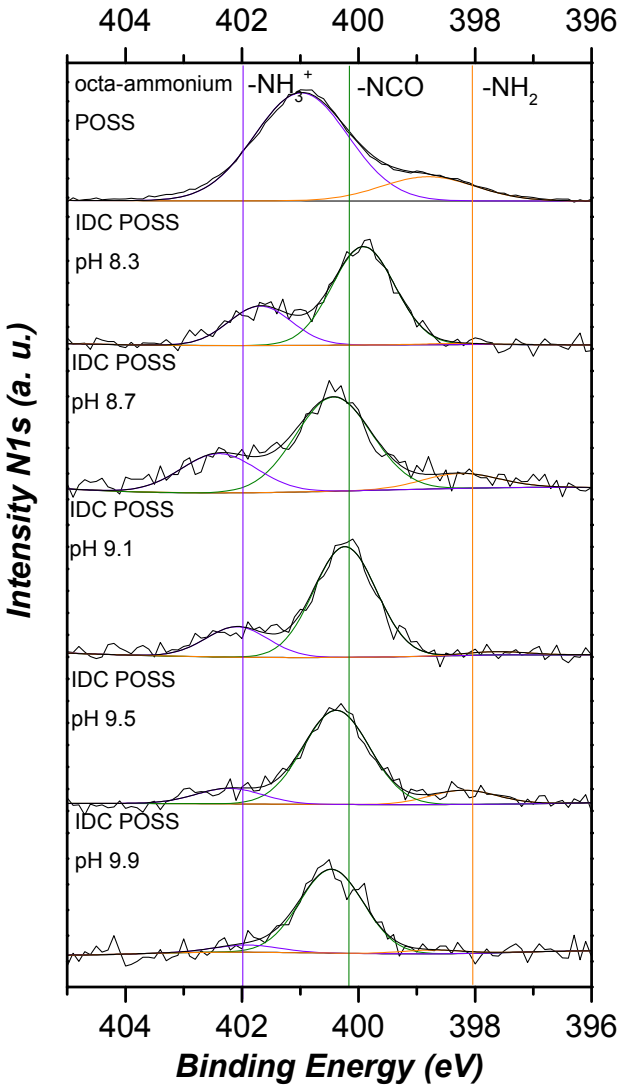

Figure 17: Comparison of XPS high resolution N1s scans of octa-ammonium POSS (top) and membranes synthesized at different pH values (pH 8.3, 8.7, 9.1, 9.5, 9.9; reaching from top to bottom). Binding energies of 398.8 eV and 400.9 eV associate with a partially deprotonated ammonia groups (NH_2 –) and the ammonia groups (NH_3^+ –). The peak at 399.77 eV originates from the amide bond (NCO –). The chemical shift of ~0.2 ev between peaks of the polyPOSS amide and octa-ammonium POSS spectrum results from the use of different XPS analysis equipment.

Figure 18 visualizes the number of ammonia groups with changing synthesis pHs. The figure shows the concentration of ammonia groups as a function of the synthesis pH of the polyPOSS amide membranes. The concentration is equivalent with the integrated peak area of the number of residual ammonia groups on each POSS cage and decreases with increasing pH. The data shows a large decline in ammonia groups form pH 8.3-9.5 from almost 30% to approximately 10% of the nitrogen in ammonia groups of the total amount nitrogen present. The higher the pH value, the more reactive amine groups can react and thus, less positive charges are on the membrane. Starting from the membrane with pH 9.5 there seems to be a constant behavior. This can be rationalized by a large amount of ammonia groups that were functionalized to primary amine groups. Most likely all amine groups react in the polycondensation reaction and this explains the consistency of the ammonia groups of membranes prepared from pH 9.5 and 9.9. It might be that few ammonia groups remain on the membrane because the POSS cage starts hydrolyzing before activating the last ammonia groups. A total absence of ammonia groups for pH 9.5 and 9.9 is also possible due to estimations in baseline corrections and signal-to-noise detection limits. The intensity of nitrogen high resolution scans is usually less compared to other elements since the photoelectron cross-sectional area is lower. However, the standard error in the peak fit is < 4 % and thus the trend indicated in the data is expected to be reliable. The error in the peak fit of ammonia concentration of IDC POSS membrane synthesized at pH 9.9 is about 30 % which designate that this peak fit is unreliable and thus ammonia groups might be absent.

In brief, these two figures indicate that part of the hypothesis is confirmed. The N1s peak analysis showed that positive charges on polyPOSS amide membranes increase systematically as the synthesis pH of the membranes decreases.

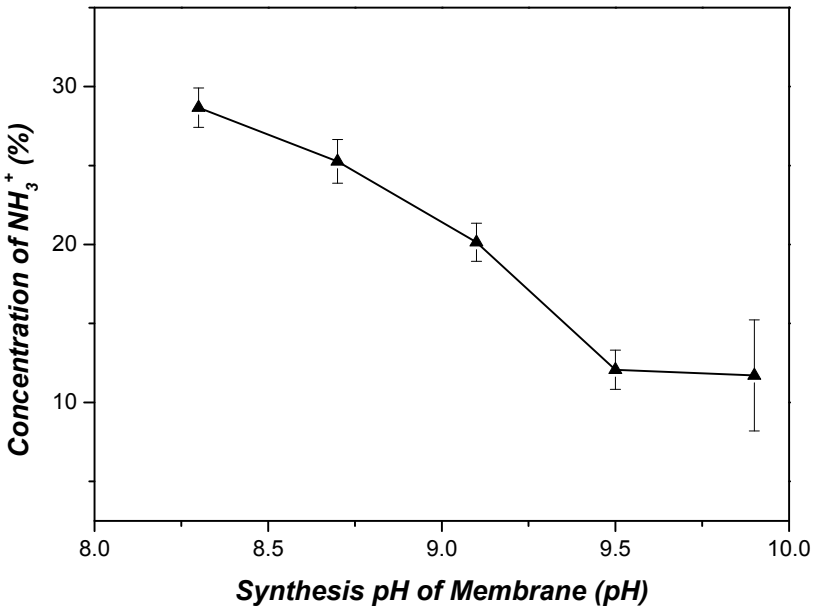

Figure 18: Concentration of ammonia groups as a function of the synthesis pH of IDC POSS membranes. The error bars indicate the standard error in the peak fitting.

Degree of Cross-Linking

Next to the results of the IR spectra, Figure 19 verifies the second part of the hypothesis of rising degree of cross-linking with increasing synthesis pH of the membrane. This is supported by the O1s peak analysis, see Appendix B, Figure 27. Figure 19 shows the functional groups consumed per POSS cage as a function of the pH at which membranes were synthesized. Two lines are depicted for comparison. The black line represents the actual number of groups which participate in the polymerization reaction as a function of synthesis pH of each membrane. The number of amine groups converted to amide groups was calculated from the percentage peak area of the amide peaks. The red line serves as reference and refers to the OH^- consumed per octa-ammonium POSS molecule as a function of pH value. This was deduced from the titration curve, see Figure 6.[1] The number of ammonia groups converted (black line) follows the general trend of increase as the titration curve (red line) suggests. While the titration curve demonstrate a smooth increase in cross-linking, the black line shows a slightly deviating behavior. The number of reacted groups range from 5-6 for pH 8.3-8.7 and from 6-8 for pH 9.1-9.9. The membranes synthesized at pH 8.7 and 9.1 show a slight variation from this behavior. The trend-breakers of pH 8.7 and 9.1 might be attributed to some residual amine groups on the POSS cages. The unreacted amine groups in those membranes might be resulting from slightly different reaction times. Alternatively, another reason for non-reacted amine groups might result from insufficient diffusion of IDC molecules in the organic phase.

When comparing the cross-linked groups (black line) of IDC POSS membranes with the number of expected groups reacted (red line) from the titration curve; in total a more functional groups have reacted (black line) than expected (red line). This unexpected behavior might originate from either measurement errors or a higher reactivity in the reaction. These findings might suggest that polycondensation reactions might occur at POSS solution pHs lower than pH 8.3.

The number of functional groups that are cross-linked per POSS cage does not directly relate to the chain length or if a homogeneous hyper cross-linked network was synthesized. It only demonstrates that more amide groups per POSS molecule are present. In any case, it is assumed that a hyper cross-linked network was created due to the high reactivity of the two components (functionalized octa-ammonium POSS and IDC).

In conclusion, a higher degree of cross-linking per POSS molecule is caused by an increase in reactive groups induced by higher pH values in the synthesis of the membrane.

[1] The expected amount of amine groups present in the octa-ammonium POSS obtained from the XPS peak analysis of octa-ammonium POSS was added to the titration data.

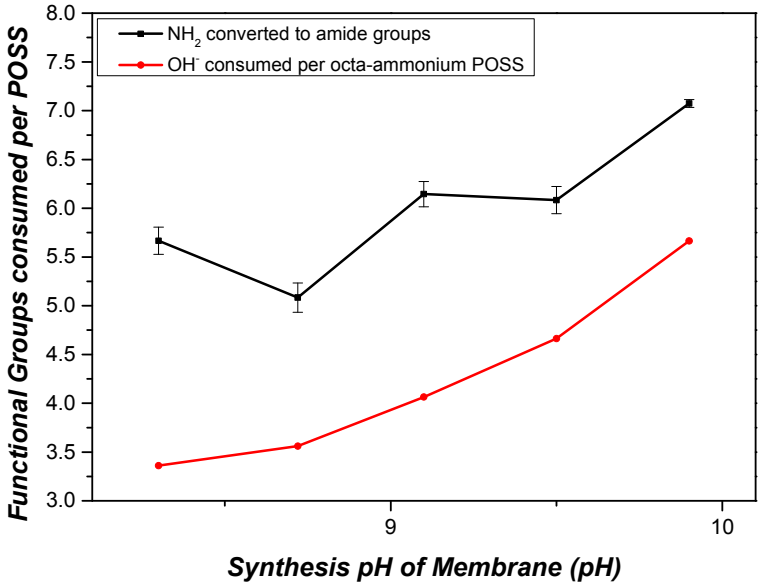

Figure 19: Functional groups consumed per POSS cage in reaction as a function of synthesis pH of IDC POSS membranes. The red line is the number of hydroxyl ions (OH^-) consumed per octa-ammonium POSS molecule while the black line shows number of primary amine groups converted to amide groups per POSS molecule. The error bars in the black line are based on standard errors in peak fitting.

Negative Charges on Membranes

Figure 20 shows that there are hardly any negative charges on the membranes since the contribution of the carboxylic acid concentration is less than 3 % for each membrane. Figure 20 compares the C1s peaks of octa-ammonium POSS as a reference and the membranes synthesized at different pHs. The octa-ammonium POSS spectrum identifies peaks at 284 eV, 284.8 eV, 285.97 eV and 287.63 eV which belong to C-NH_3^+, C-C, C-Si and C-NH_2 groups. In the polyPOSS amide spectra additional peaks at 288.11 eV and 289.5 eV appear due to the N-C=O bonds and acidic groups (COOH). Acidic groups arise from side reactions of non-reacted acyl chloride groups. Again the XPS spectra of octa-ammonium POSS and polyPOSS-amides in Figure 20 have slight shifts that can be rationalized by different XPS analysis equipment used. The chemical shifts within the polyPOSS-amide spectra appear due to different counter ions present.

Further, Figure 20 shows the highest contribution with 2.6 % of the carboxylic acid group is in the membrane synthesized at pH 8.7. Although, it should be noted that acidic gorups could also not be present due to incorrect estimations in base line settings and signal-to-noise ratios larger than 3. Therefore, the anticipation of little amounts of carboxylic acid groups present is confirmed. The low amount of negative charges is governed by the reactivity of the IDC cross-linker because the architecture of IDC molecules exhibits a low steric hindrance and thus less side-reactions occur.

The C-NH_3^+ peak has also only minor contribution which is attributed to the high intensity of the C-C and C-Si peaks. The C-C and C-Si peaks, of polyPOSS amide spectra with a slight chemical shift of max. 0.2 are analyzed in the next figure. The C-NH_2 peak is not visible in those spectra since it was not possible to fit it at the point where C-Si and N-C=O peaks overlap. In the N1s spectra (Figure 17) it was already shown that their fraction is only minor.

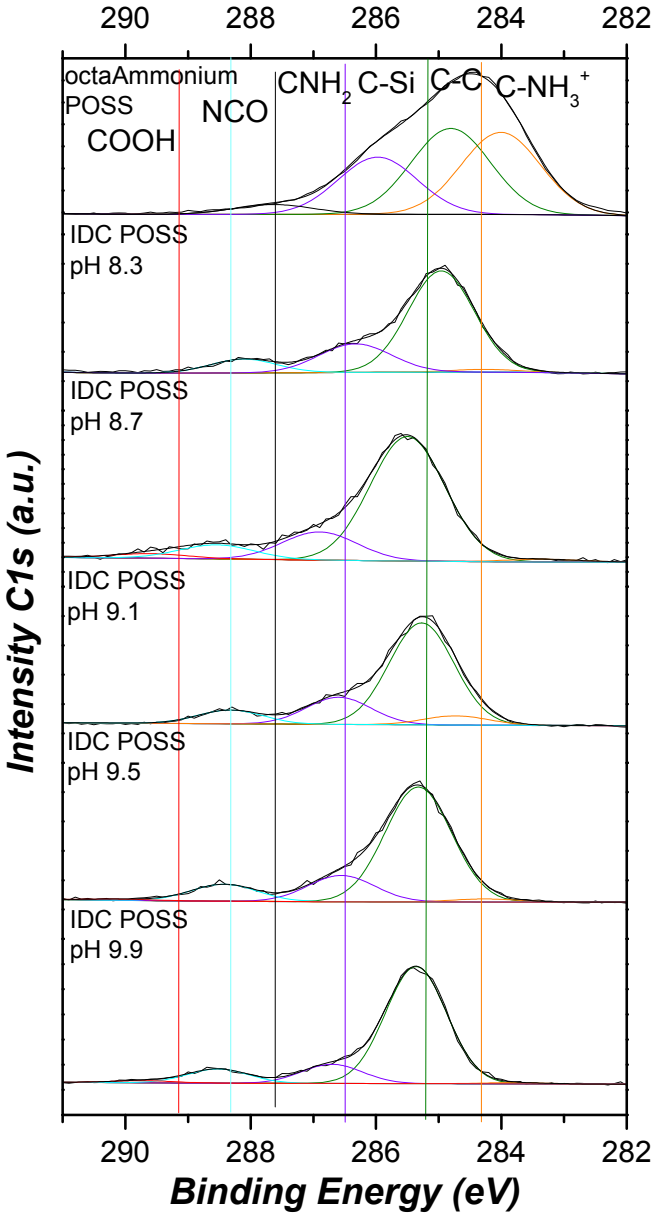

Figure 20: Comparison of XPS high resolution C1s scans of octa-ammonium POSS and membranes synthesized at different pHs (pH 8.3, 8.7, 9.1, 9.5, 9.9 reaching from top to bottom). The octa-ammonium POSS spectrum identifies peaks at 284 eV, 284.8 eV, 285.97 eV and 287.63 eV which belong to C-NH_3^+ –, C-C –, C-Si – and CNH_2 – groups. In the polyPOSS amide spectra additional peaks at 288.11 eV and 289.5 eV appear due to the C-N=O – groups and acidic groups (COOH –). The chemical shift of ~0.2 ev between the polyPOSS amide and octa-ammonium POSS spectrum results from the use of different XPS analysis equipment.

The analysis of the peak ratios of C-C to C-Si supports the increment in degree of cross linking with increasing preparation pH of membranes. Figure 21 shows an indicator of degree of cross-linking as a function of synthesis pH of membrane. The red line is the titration data, depicting the OH- consumed per POSS cage as a function of preparation pH of the membrane and serves as reference. The black line shows the ratio of integrated peak area of C-C and C-Si of the experimental XPS data versus the synthesis pH of the membrane. Both lines follow the same trend, rationalizing the expected increase in degree of cross linking. The logarithmic incline of peak ratios of C-C to C-Si (black line) was anticipated.

On one hand, the C-C IDC POSS peak area increases in comparison to the C-C POSS peak since the phenylring of the IDC molecule owns a binding energy at the same position as the C-C bond (~284.66 eV). Therefore, the peak area of C-C in IDC POSS is expected to rise with respect with increasing synthesis pH because more IDC molecules are cross-linked. On the other hand, the Si-C peak area should decrease with higher syntheis pH values of polyPOSS membranes since POSS cages are involved in more bonds. This finally reduces peak intensity of the C-Si peaks with increasing pH values.

The rising trend of integrated peak area ratios is supported by the elemental ratios of C to Si which show the same behavior (Appendix C, Figure 28). Both graphs show the same trend-breaker at pH 8.7. The trend breaking of pH 8.7 was already seen from other XPS spectra. Most likely it is associated with the membrane sample meaning either a contaminated sample or errors in the synthesis. There are several issues in the membrane preparation e.g. contaminants, leaking of the membrane in impregnation steps etc.

To summarize, the comparison of the C1s peaks demonstrates that the architecture of the IDC molecule allows high conversion of the acyl chloride groups and thus low amount of negative charges. Furthermore, the peak ratio analysis of C-C and C-Si underlines that the degree of cross-linking increases logarithmically with increasing synthesis pH of the membrane.

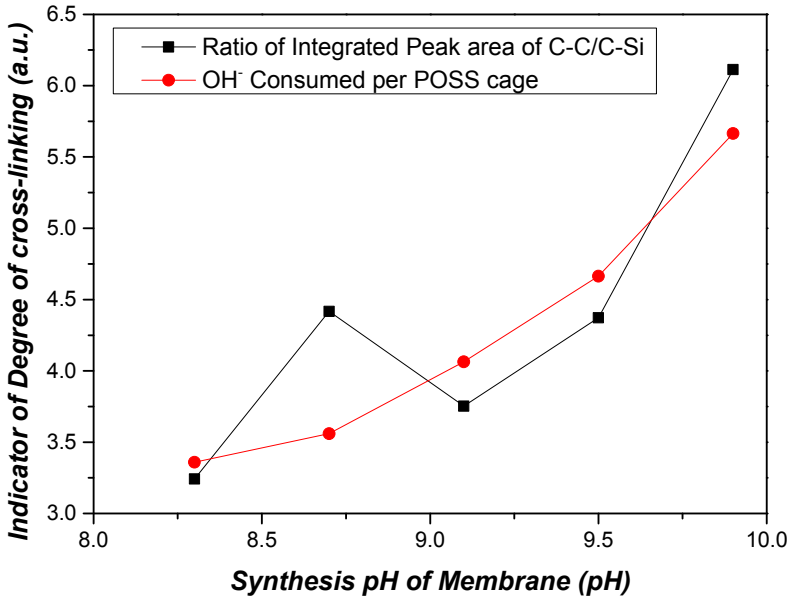

Figure 21: Indicator of degree of cross-linking as a function of synthesis pH of IDC POSS membranes. The red line is refers to the OH^- consumed per POSS cage as a function of preparation pH of the membrane (reference) expected. The black line shows the ratio of integrated peak area of C-C and C-Si of the experimental XPS data as a function of the synthesis pH of the IDC POSS membranes.

4.2.3 Streaming Zeta Potential

Synthesized membranes were positively charged below pH 8, indicated by the isoelectric points of the polyPOSS amide membranes that are scattered around pH 8. Figure 22 shows zeta potential as a function of pH of titration solutions for each membrane synthesized at different pH values (differently colored) and the PAN support (grey line) including 95 % confidence interval. All polyPOSS-amide graphs have a similar shape with first high zeta potentials and at some point it drops to negative zeta potentials. As expected solutions with lower pH tend to increase zeta potentials of

surfaces and own positive zeta potentials for low pH values. Similarly, adding of a basic solution lowers the zeta potential and thus a decreasing behavior with increasing pH is shown as expected. However, the line of the polyPOSS-amide prepared at pH 9.1 shows odd behavior in the beginning and should therefore be repeated. The zeta potential of the PAN support is negative over the entire pH range measured (pH 4-10). The negatively charged PAN support can influence the zeta potential measurements since IDC POSS membranes are water permeable. Therefore, interpretations of absolute values cannot be directly translated to surface charge.

The charges on membranes in neutral environment (pH 7) are particularly interesting since many membrane separations are executed in neutral environments. From Figure 22 it can be seen that all membranes are positively charged around pH 7. Figure 30 in Appendix D depicts the exact values of the zeta potential of different IDC POSS membranes in neutral pH environment, although no trends can be deduced from it. Membranes synthesized at pH 9.9 and 9.5 show a large amount of positive charges. This behavior is associated with a higher degree of cross- linking in membranes prepared at high pH and thus the PAN support is influencing. Therefore, the zeta potential is reduced less.

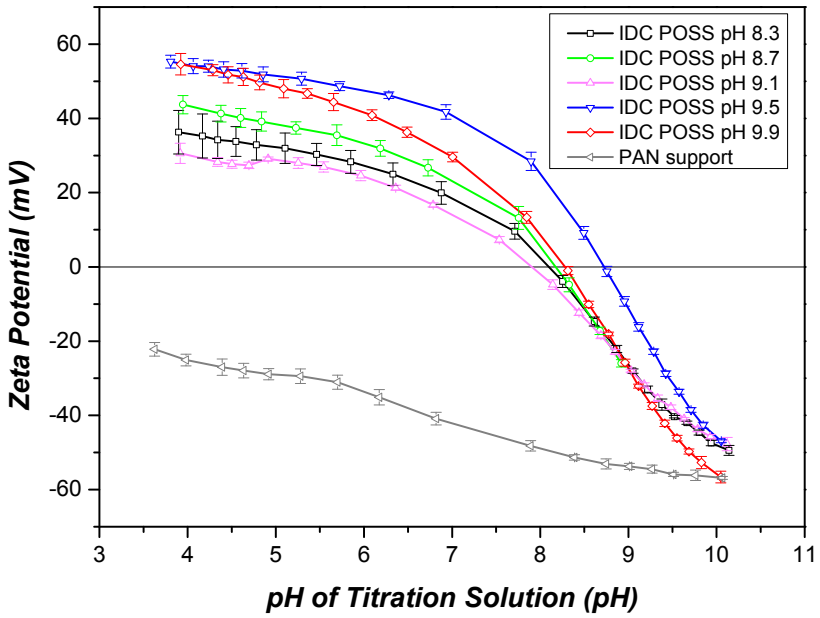

Figure 22: Zeta potential as a function of pH of titration solution for IDC POSS membranes synthesized at different pHs (pH 8.3 –, 8.7 –, 9.1 –, 9.5 –, 9.9 –) and the PAN support (–) as reference spectrum. The error bars show the 95% confidence interval.

The isoelectric points of polyPOSS amides scatter around pH 8 as shown in Figure 23, correlating with a slightly positively charged membrane below pH 8. When the zeta potential reaches zero, the IEP is achieved, meaning that charges are neutralized. As explained in the theory section the IEP is characterized by the pKa values of the functional groups present. The pKa of carboxylic acid groups (COOH) and for the ammonium groups (NH_3^+) are at pKa 5 and pKa 10, respectively [48]. Figure 23 shows the IEPs versus the pH at which membranes were synthesized, including error ranges 95% CI as a function of pH. Figure 23 does not confirm any trend as a function of synthesis pH. This is due to the fact that IEPs do not depend on amount of type of functional group present but on ratio of which different types of groups are present (COOH to NH_3^+). The IEPs of IDC POSS membranes are closer to pH 10 due to a larger contribution of ammonia groups compared to carboxylic acid groups. Absolute

values cannot be interpreted due to inaccuracy in streaming potential measurements originating from electrolyte concentrations and PAN support influences.

Further, the Figure 23 shows that all IEPs are around pH 8 except the polyPOSS amide membrane synthesized at pH 9.5 with an IEP at pH 8.7. The exceptional high IEP of the membrane synthesized at pH 9.5 was measured twice and both measurements resulted in same high IEPs. This suggests that the membrane is responsible for the high IEP and not measurement errors or differing electrolyte concentrations. One possible explanation is that the layer of the polyPOSS amide film which was produced was thicker and more cross-linked. That would mean that the PAN support is less influencing the streaming zeta potential and IEPs are closer to the present pKas of the present NH_3^+. However, another IDC POSS sample synthesized at pH 9.5 (see Appendix D, Figure 29) showed an IEP of pH 8, suggesting that the previous zeta potential data of IDC POSS sample are exceptional.

In essence, the IEPs of polyPOSS amides demonstrate that positive charges are present on the membrane. Membranes synthesized with TMC by Mitchel Noijen (Bachelor student, Inorganic Membranes) [20] only show IEPs around pH 6. This is explained by the fact that the IDC owns a better reactivity due to less steric hindrance compared with TMC. As a result less carboxylic acid groups are present, leading to higher IEPs.

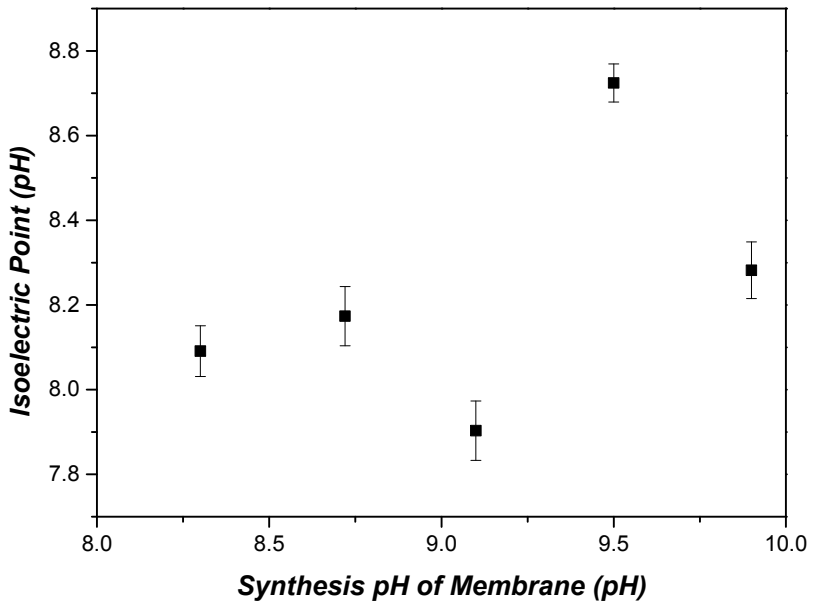

Figure 23: Isoelectric points for IDC POSS membranes as a function of synthesis pH value of IDC POSS membranes.

From the streaming potential data it can be concluded that membranes are positively charged below pH 8. However, the IEP values cannot be considered as absolute since negatively charged PAN support is affecting the measurements. Thus, the thickness and degree of cross linking of polyPOSS film has also an influence. Therefore, it is useful to determine the zeta potential using different techniques and to determine the morphology of the membranes. The next technique applied to determine zeta potentials was contact angle pH titration.

4.2.4 CONTACT ANGLE PH TITRATION

In this study, the technique of contact angle pH titration to characterize surface charges failed. The results from contact angle pH titrations are shown in Appendix E, Figure 31. The figure depicts the contact angles in degree as a function of pH of the titration solutions. The results only show scattered data varying from 80°-100° for all IDC-POSS membranes synthesized. This data solely indicates that IDC POSS membranes might be slightly hydrophobic in nature. That means that IDC-POSS membranes might be sensitive to fouling induced by organic compounds. The failure of that method might be caused by several factors. External errors include incorrect base line settings or inaccuracy in measuring time but these are assumed to have minor contribution. More influencing are surface morphologies (i.e. surface roughness and layer thickness) and external influences as permeation of droplets into membranes and instability of solutions with pH values around pH 7. Conclusively, contact angle pH titration failed and needs to be optimized for the use in zeta potential characterization.

5. CONCLUSION

This study investigated the manners of positive charges and degree of cross-linking of hybrid polyPOSS-amide membranes as a function of the pH of the POSS solution. ATR-FT-IR and XPS analysis confirms that a hybrid polyPOSS amide network was synthesized by IP. Inorganic POSS cages were covalently linked by aromatic amide bridges to organic moieties. Therefore, a film which is suggested to be flexible and robust at the same time was synthesized.

All IDC POSS membranes synthesized were positively charged below pH 8. This was rationalized by high reactivity of IDC towards cross-linking with POSS cages and thus a low amount of acidic groups on the IDC POSS membranes, supported by XPS data (C1s spectrum). However, exact values from streaming zeta potential measurements are not very reliable mainly due to influences of electrolyte concentration and PAN support. Therefore, more methods to characterize surface charges are needed. A trend of more positive charges for lower pH in preparation and similarly more cross-linking for membranes with higher pH values was confirmed by ATR-FT-IR and XPS analysis. There is a larger amount of positive charges present, especially for membranes synthesized at lower pH (pH 8.3-9.1).

Further, an increase in cross-linking with simultaneous increase in hydrolysis of POSS cages was deduced from ATR-FT-IR data. These facts are particularly important for later permeation experiments and analysis of further measurements. In any case, the characterization showed that the objective was achieved to change systematically positive charges in the hybrid IDC-POSS membranes.

The applicability in textile industry needs to be examined with permeation experiments with different cationic dyes and IDC-POSS membranes. The separation of cationic dyes from water might suffer from merely low contribution of positive charges. However, NF membranes also separate partially by molecular size exclusion. In addition, IDC-POSS membranes suggest having promising thermal-mechanical stability which is suitable for harsh conditions in textile effluents. Salt retention experiments should enlighten fouling properties of polyPOSS amide membranes which are surmised to be sensitive to organic fouling agents.

6. RECOMMENDATIONS

The current study gave insight about charge character of IDC-POSS membranes. The results indicate that lower synthesis pH of the POSS solution led to an increase in positive charges on the polyPOSS amide membranes. In order to manifest and strengthen the validity of this trend, the reproducibility has to be evaluated by synthesis and characterization of more sets of IDC POSS membranes.

6.1 ADDITIONAL MEASUREMENTS

The zeta potential needs to be determined by additional techniques which might be more reliable. One opportunity is to optimize contact angle pH titration by using for example charged surfactants as suggested by Rosa et al [45] or direct titration by dyes [29].

Morphology and homogeneity of polyPOSS amide membranes should be examined to complete characterizations of IDC POSS membranes. This can be employed by Atomic Force Microscopy (AFM). The determination of morphology and homogeneity of polyPOSS amide films would help in explaining for example deviations in IEPs between different membranes. In addition, morphology and homogeneity have an impact on membrane performance. It is suggested that membranes prepared at lower pH would have a more open structure due to less cross-linking; this proposes higher fluxes. In addition, polyPOSS amide films synthesized at lower pH values might have a higher homogeneity because of less hydrolysis of POSS cages. The active layer thickness could be determined by scanning electron microscopy (SEM). The thickness is anticipated to be similar for every membrane due to same reaction times.

Furthermore, NF experiments of all IDC POSS membranes are inevitably necessary to conclude the general performance of the membranes regarding fouling, selectivity and fluxes. For applicability of IDC POSS membranes in dye separation, it is advisable to employ salt retention and permeation measurements cationic dyes. Carmen et al [49] give an overview of cationic dyes which can be potentially used e.g. methylene blue. According Donnan-exclusion principle it is assumed that IDC POSS membranes with a higher positive charge density should provide a higher rejection of multivalent cations. Therefore, membranes synthesized at lower pH are assumed to have a higher rejection of multivalent cations. All IDC POSS membranes are expected to be fouling sensitive to organic matter. Contrarily, the antifouling properties to calcium bridging to alginates should increase with decreasing preparation pH. However, it is difficult to predict the performance since membrane performance also depends on defects in the membrane, density and several synthesis parameters.

6.2 FOLLOW-UP STUDY

XPS results (N1s peaks) indicate that activation of the POSS cages was higher than predicted from the titration data. This might be an error in the measurement data. On the other hand, it might suggest that the polycondensation reaction occur at preparation pHs even lower than pH 8. Therefore, membranes prepared with pHs below pH 8 can be synthesized with anticipations of higher positive charges on the membranes compared to membranes synthesized at pH 8.3.

Another follow-up study might be to test more cross linkers e.g. p-Phthaloyl dichloride or BHAC. The polyPOSS-amide membranes with cross-linker of TMC or IDC own IEPs of pH ~6 and ~8, respectively. It is assumed that the amount of negative charges changes with respect to the degree of hindrance of the acyl chloride groups. Conclusively, less sterically hindered groups might lead to less acidic groups on the membranes and a higher charge density of positively charges.

ACKNOWLEDGEMENTS

First and foremost, I have to thank my supervisors Michiel Raaijmakers and Evelien Maaskant. I am grateful for your support and time for discussions etc. throughout my entire bachelor assignment. It was a pleasure working with two professional and very critical persons who were giving a lot of valuable input to improve my thesis. I would also like to show gratitude to my examination committee, including prof. dr. ir. Nieck Benes, dr. ir. Herbert Wormeester, ir. Michiel Raaijmakers, ir. Evelien Maaskant and dr.ir. Wojciech Ogieglo. I am thankful that Nieck who was one my professors in the third year, raised my interest in this bachelor assignment which I enjoyed a lot. Furthermore, I appreciate that Wojciech agreed on being part of my examination committee and thus accepted additional work load. It was a pleasure of being part of the Inorganic Membrane Group which is a very enjoyable and inspiring team. I wish all group members great success with future research.

7. REFERENCES

1. Cheng, S., et al., *Positively charged nanofiltration membranes: Review of current fabrication methods and introduction of a novel approach.* Advances in Colloid and Interface Science, 2011. **164**(1-2): p. 12-20.
2. Mulder, M., *Basic Principles of Membrane Technology*. second edition ed. 1996, The Netherlands: Kluwer Academic Publishers.
3. Benes, N., *Scheidingsmethoden, Membrane Technology*. 2013.
4. Dalwani, M., et al., *Ultra-thin hybrid polyhedral silsesquioxane-polyamide films with potentially unlimited 2D dimensions.* Journal of Materials Chemistry, 2012. **22**(30): p. 14835-14838.
5. Lint de, W.B.S., et al., *Ion Adsorption Parameters Determined from Zeta Potential and Titration Data for a y-Alumina Nanofiltration Membrane*. 2003, American Chemical Society.
6. Liu, J., L. Yu, and Y. Zhang, *Fabrication and characterization of positively charged hybrid ultrafiltration and nanofiltration membranes via the in-situ exfoliation of Mg/Al hydrotalcite.* Desalination, 2014. **335**(1): p. 78-86.
7. Wang, T., et al., *A novel highly permeable positively charged nanofiltration membrane based on a nanoporous hyper-crosslinked polyamide barrier layer.* Journal of Membrane Science, 2013. **448**(0): p. 180-189.
8. Li, X., et al., *Biomass and Carbon Storage in an Age-Sequence of Korean Pine (Pinus koraiensis) Plantation Forests in Central Korea.* Journal of Plant Biology, 2011. **54**(1): p. 33-42.
9. Du, R. and J. Zhao, *Properties of poly (N,N-dimethylaminoethyl methacrylate)/polysulfone positively charged composite nanofiltration membrane.* Journal of Membrane Science, 2004. **239**(2): p. 183-188.
10. Lang, W.Z., et al., *The roles of alkali metal counter-ions of PFSA play in the formation of PVDF/PFSA-M hollow fiber membranes.* Desalination, 2012. **292**: p. 45-52.
11. Lang, W.Z., et al., *Preparation and characterizations of charged poly(vinyl butyral) hollow fiber ultrafiltration membranes with perfluorosulfonic acid as additive.* Journal of Membrane Science, 2013. **430**: p. 1-10.
12. Peng, W. and I. Masanao, *Novel Biopolymer Composite Membrane Involved with Selective Mass Transfer and Excellent Water Permeability*. 2012.
13. Mukherjee, P., K.L. Jones, and J.O. Abitoye, *Surface modification of nanofiltration membranes by ion implantation.* Journal of Membrane Science, 2005. **254**(1–2): p. 303-310.
14. Freger, V., J. Gilron, and S. Belfer, *TFC polyamide membranes modified by grafting of hydrophilic polymers: an FT-IR/AFM/TEM study.* Journal of Membrane Science, 2002. **209**(1): p. 283-292.
15. Lee, J., A. Hill, and S. Kentish, *Formation of a thick aromatic polyamide membrane by interfacial polymerisation.* Separation and Purification Technology, 2013. **104**(0): p. 276-283.
16. Solutions, D.w.P. *Products- Filmtec NF270-400/34i*. [cited 2014 5.5.]; Available from: http://www.dowwaterandprocess.com/en/products/f/filmtec-nf270-400-34i.
17. Cadotte, J.E., et al., *Interfacial synthesis in the preparation of reverse osmosis membranes.* Journal of Macromolecular Science—Chemistry, 1981. **15**(5): p. 727-755.
18. Lau, W.J., Ismail A.F., *Progress in Interfacial Polymerization Technique on Composite Membrane Preparation.* International Conference on Environmental Engineering and Applications, 2011. **17**.
19. Lau, W., et al., *A recent progress in thin film composite membrane: a review.* Desalination, 2012. **287**: p. 190-199.
20. Noijen, M., *Hybrid Polyhedral Oligomeric Silsesquioxanes/ Trimesoyl Chloride Membranes for Solvent Nanofiltration*, in *Inorganic Membranes*. 2013, University of Twente: The Netherlands, Enschede.
21. Plastics, H. [cited 2014 10.06.]; Available from: http://www.hybridplastics.com/products/am0285.htm.

22. Mo, Y., et al., *Improved Antifouling Properties of Polyamide Nanofiltration Membranes by Reducing the Density of Surface Carboxyl Groups.* Environmental Science & Technology, 2012. **46**(24): p. 13253-13261.
23. Hermans, S., *Membranes synthesized via interfacial polymerization: from aqueous to solvent resistant nanofiltration*, in *Faculty of Bioscience Engineering*. 2014, KU Leuven.
24. J. Feher, F., et al., *Syntheses of highly functionalized cube-octameric polyhedral oligosilsesquioxanes (R8Si8O12).* Journal of the Chemical Society, Dalton Transactions, 1999(9): p. 1491-1498.
25. Ogieglo, W., et al., *n-Hexane induced swelling of thin PDMS films under non-equilibrium nanofiltration permeation conditions, resolved by spectroscopic ellipsometry.* Journal of Membrane Science, 2013. **437**(0): p. 313-323.
26. Cheng, S., et al., *Characterisation and application of a novel positively charged nanofiltration membrane for the treatment of textile industry wastewaters.* Water Research, 2012. **46**(1): p. 33-42.
27. Berta, D., et al., *Bifunctional Polymer-Metal Nanocomposite Ion Exchange Materials*. 2012.
28. Xu, Y. and R.E. Lebrun, *Investigation of the solute separation by charged nanofiltration membrane: effect of pH, ionic strength and solute type.* Journal of Membrane Science, 1999. **158**(1–2): p. 93-104.
29. Tiraferri, A. and M. Elimelech, *Direct quantification of negatively charged functional groups on membrane surfaces.* Journal of Membrane Science, 2012. **389**(0): p. 499-508.
30. Nath, K., *Membrane Separation Processes*. 2008, New Delhi-110001: Asoke K. Ghosh, Prentice-Hall of India Privete Limited, M-97.
31. Hurwitz, G., G.R. Guillen, and E.M.V. Hoek, *Probing polyamide membrane surface charge, zeta potential, wettability, and hydrophilicity with contact angle measurements.* Journal of Membrane Science, 2010. **349**(1–2): p. 349-357.
32. Ostuni, E., et al., *A Survey of Structure–Property Relationships of Surfaces that Resist the Adsorption of Protein.* Langmuir, 2001. **17**(18): p. 5605-5620.
33. Cui, X.C., K.-H., *Natural Organic Matter Removal and Fouling Control in Low-Pressure Membrane Filtration for Water Treatment FAU - Cui, Xiaojun FAU - Choo, Kwang-Ho.* Environ Eng Res, 2014. **19**(1): p. 1-8.
34. Atkins, P., *Physical Chemistry*. 2010: OXFORD. 972.
35. Hofstetter, H., *FT-IR Spectroscopy Attenuated Total Reflectance*. 2007.
36. Physical Electronics; Available from: https://www.phi.com/contact.html.
37. Briggs, D., *Surface Analysis of Polymers by XPS and Static SIMS*, ed. C.U. Press. 1998.
38. Roger Smart, S.M., Mike Bancroft, Igor Bello, *X-ray Photoelectron Spectroscopy*.
39. Laurin, M. *Principle of X-ray photoelectron spectroscopy* 2009; Available from: http://www.texample.net/tikz/examples/principle-of-x-ray-photoelectron-spectroscopy-xps/.
40. Barnes, G.T.G., I. R., *Interfacial Science*. second ed. 2011, United States: Oxford University Press Inc. New York.
41. Yoon, S., *Electric Double Layer According to Stern Model*. after Shaw 1969.
42. Calgary, U.o.; Available from: http://www.chem.ucalgary.ca/courses/351/Carey5th/Ch27/ch27-1-4.html.
43. Xie, H., T. Saito, and M.A. Hickner, *Zeta Potential of Ion-Conductive Membranes by Streaming Current Measurements.* Langmuir, 2011. **27**(8): p. 4721-4727.
44. Hurwitz, G., G.R. Guillen, and E. Hoek, *Probing polyamide membrane surface charge, zeta potential, wettability, and hydrophilicity with contact angle measurements.* Journal of Membrane Science, 2010. **349**(1): p. 349-357.
45. Rosa, M. and M. De Pinho, *Membrane surface characterisation by contact angle measurements using the immersed method.* Journal of membrane science, 1997. **131**(1): p. 167-180.

46. Jenkinson, D. *Contact Angles of Hydrophobic and Hydrophilic Surfaces*. 2013; Available from: http://danthechemist.files.wordpress.com/2013/02/ca2.jpg.
47. Socrates, G., *Infrared and raman characteristic group frequencies : tables and charts*. 2001, Chichester [etc.]: Chichester etc. : Wiley.
48. Bruice, P.Y., *Organic Chemistry*. seventh ed. 2014, United States of America.
49. Carmen, Z. and S. Daniela, *Textile Organic Dyes–Characteristics, Polluting Effects and Separation/Elimination Procedures from Industrial Effluents–A Critical Overview.* ISBN, 2012: p. 978-953.

APPENDICES

APPENDIX A- POLYCONDENSTAION REACTION

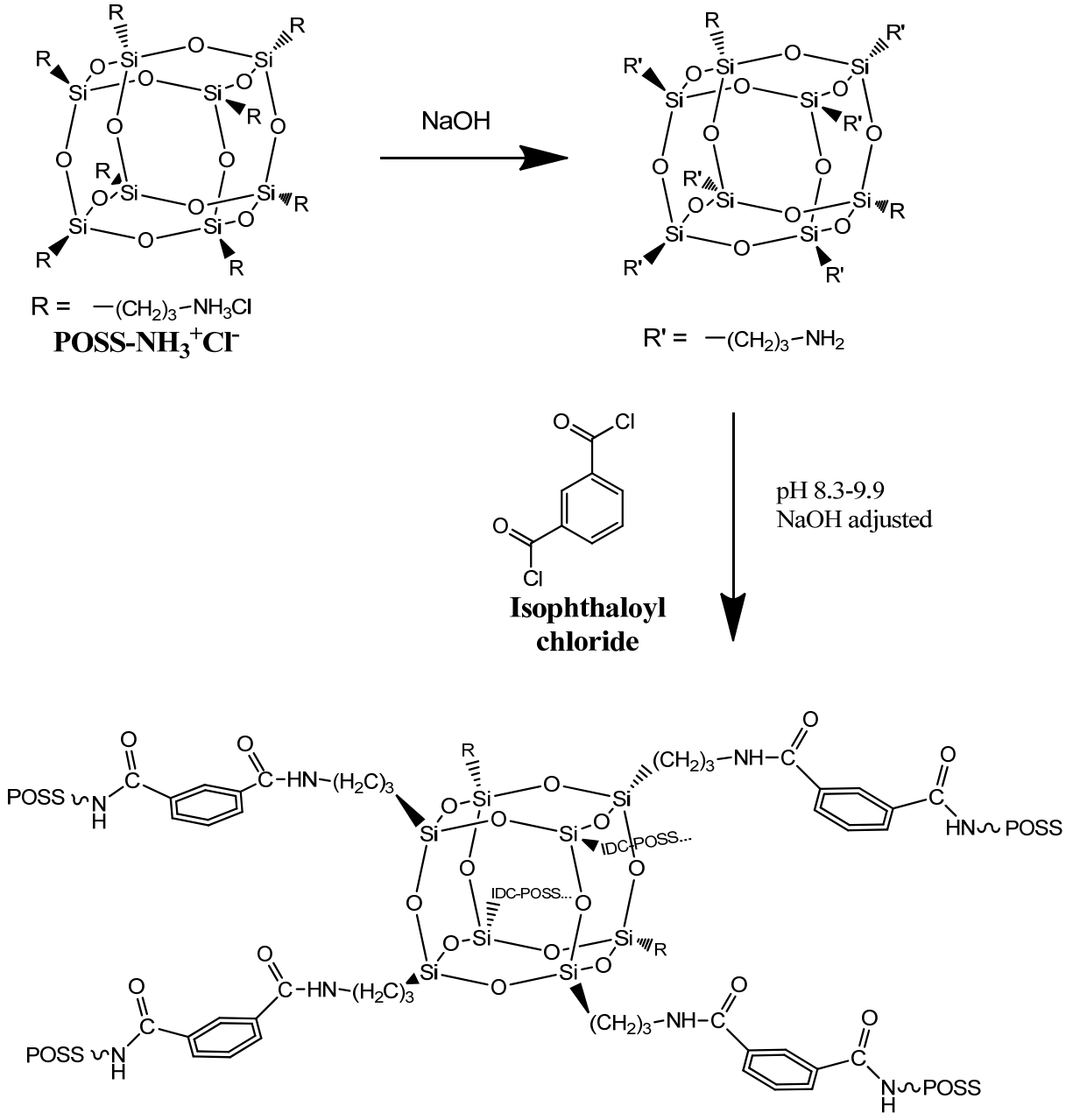

Figure 24: Reaction scheme of the interfacial polymerization. In the first step octa-ammonium groups of POSS cages are partially deprotonated, resulting in reactive primary amine groups. The amine groups react in a polycondensation reaction with IDC through which the subsequent network is formed.

APPENDIX B- ATTENUATED TOTAL REFLECTION-INFRARED SPECTROSCOPY

Table 2: Infrared peak analysis for functional groups expected in the IDC POSS membranes.

Functional group	Stretch/Bend	Shape	Intensity[2]	Position (cm^{-1})
Amide group				
NH (sec. amide)	stretch	Sharp, doublet (cis-trans isomerism)	m m w	3370-3270 (trans) 3180-3140 (cis) 3100-3070 (trans)+ overtone 1550
NH (sec. amide)	deformation		s	1570-1515
C=O (sec. amide)	stretch		s	1680-1630
CN (sec. amide)	stretch		w-m	1305-1200 1260
Primary amines on POSS				
CN (prim. aliph. amines)	stretch		m	1120, 1130 1134, 1037
NH_2	Stretch	broad	w-m	3450-3160
NH (prim. aliph. amines)	deformation		m-s	850-810
Ammonia on POSS				
NH_3^+ (CH_2-NH_3^+)	Sym. stretch		m	3010-2910
CH_2-NH_3^+	Asym.stretch	broad	m	3235-3030
	Asym.stretch	broad	m	3115-2985
	Asym NH3+ def.		m-s	1635-1585
	Asym NH3+ def.		m-s	1615-1560
Aliphatic Carbon				
-$(CH_2)_3$-			w-m	735-725
-CH_2- (acyclic)	Asym stretch	Raised by EN substituent	m-s	2975-2950
	Sym. stretch	Raised by EN substituent	m	2870-2840
Silsequioxanes				
Si-O-Si	ladder stretch			1040
	polyhedral stretch			1125
Phenyl ring of IDC				
C=C (aromatic)	Stretch			1465, 1506, 1614
C-H (aromatic)	Stretch			3068, 3032

ATR-FT-IR SPECTRUM

The examination of positive charges was performed by XPS data analysis since no qualitative data can be obtained from the IR spectrum in Figure 25. The figure shows a close up of 3800 cm^{-1}-2200 cm^{-1} of the normalized absorbance of IDC POSS Membranes, normalized with respect to the polyhedral POSS peak at 1225 cm^{-1}. Stretching vibrations attributed to ammonia groups are overlapping with aliphatic carbon and amide vibrations in the second part of the spectrum 3800 cm^{-1}- 2200 cm^{-1}, thus no qualitative deductions can be made.

[2] w=weak, m=middle, s= strong

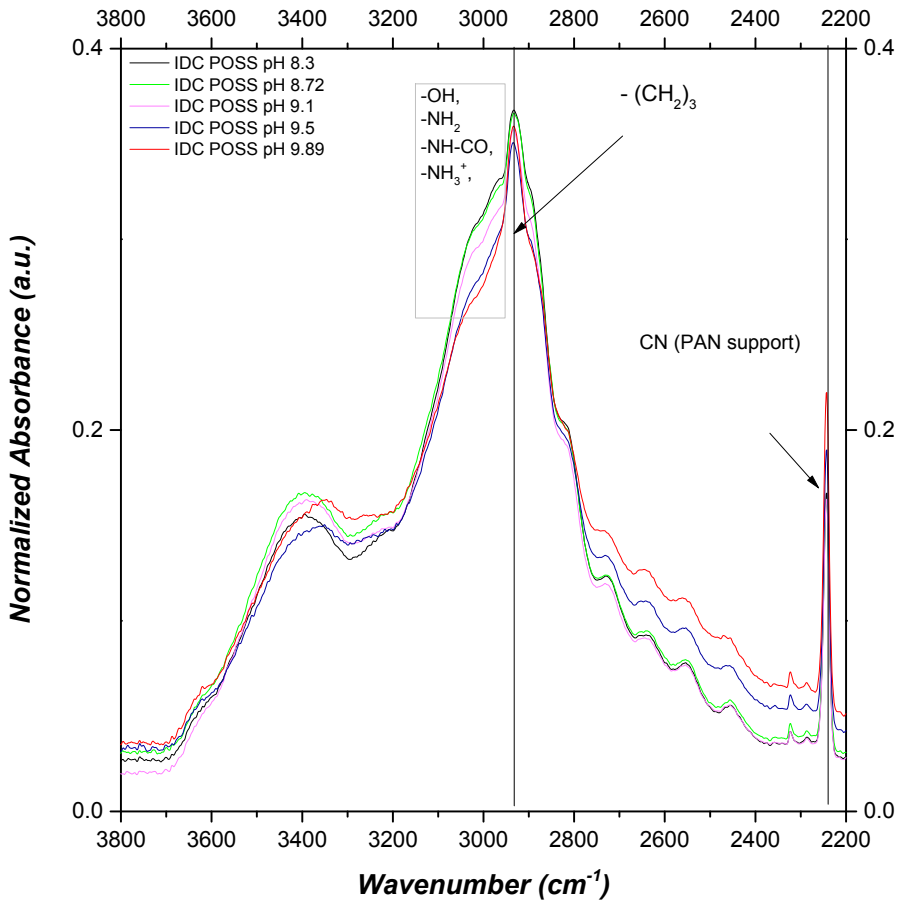

Figure 25: Normalized infrared absorbance spectra (zoom of 3800-2200 cm^{-1}) of IDC POSS synthesized at different pH values (pH 8.3 –, 8.7 –, 9.1 –, 9.5 –, 9.9 –)

APPENDIX C- X-RAY PHOTOELECTRON SPECTROSCOPY

Table 3: Elemental concentrations and ratios for octa-ammonium POSS (theoretical values) and IDC POSS membranes synthesized at different pH values obtained from XPS.

	Elemental concentration (%)					**Elemental ratio**				
	C	N	O	Si	Cl	C/N	O/Si	O/N	Cl/N	C/Si
OctaAmmonium POSS (theor.)	40	13.3	20	13.3	13.3	3	1.5	1.5	1	3
IDC POSS pH of synthesis	**Elemental concentration (%)**					**Elemental ratio**				
8.3	64.6	8.3	17.2	7.4	2.5	7.8	2.3	2.1	0.3	8.7
8.72	67.4	7.6	15.6	6.6	2.7	8.8	2.4	2.1	0.4	10.2
9.1	63.2	8.8	18.7	7.8	1.6	7.2	2.4	2.1	0.2	8.1
9.5	65.8	7.6	18.2	7.3	1.2	8.6	2.5	2.4	0.2	9.1
9.9	69.6	5.5	18.2	6.1	0.6	12.6	3	3.3	0.1	11.4

Table 4: Peak analysis for XPS of octa-ammonium POSS, IDC and expectations for IDC POSS membranes. The table shows the binding energies in (BE (eV)) and the corresponding functional group (id).

	Octa-ammonium POSS				**Isophthaloyl Dichloride**				
	C				**C**				
BE (eV)	284	284.8	285.97	287.63	287.9	289.5	288.11	284.66	287.02
id	C-NH3+	C*-C	C*-Si	C-NH2	C*=O	C*OOH	N-C=O	Phenyl ring	C-Cl
	O				**O**				
BE (eV)	531.833				532.6	532.1	531.3		
id	Si-O*-Si				SiO*H	Si-O*-Si	N-C=O*		
	Si								
BE (eV)	102.11	103.2							
id	Si*-O_3C	Si*OH							
	N				**N**				
BE (eV)	398.8	400.9			399.77				
id	C-N*H_2	-N*H_3^+			N*-C=O				

HIGH RESOLUTION SCAN SI2P

Figure 26 shows the intensity of Si2p peaks as a function of binding energy for the octa-ammonium POSS and IDC POSS spectra. The octa-ammonium POSS spectrum identifies peaks at 102.11 eV associated with SiO_3C groups. In the polyPOSS-amide spectra additional peaks at 103.2 eV emerge which are associated with the Si-OH bonds from hydrolyzed POSS cages. From low to high synthesis pH the peaks of Si-OH increase; originating from the increasing hydrolysis of POSS cages with increasing synthesis pH. Compared to ATR-FT-IR analysis the amount of cleavage of POSS cages is smaller only about 10% and larger. The data of the XPS analysis concerning hydrolysis might be more reliable compared to IR but was not included since the focus is on the charge behavior of the hybrid polyPOSS amide membranes. The trends are not directly equal and comparable because different membrane samples were used. This might indicate low reproducibility of membranes because pH 9.9 shows a decrease in hydrolysis.

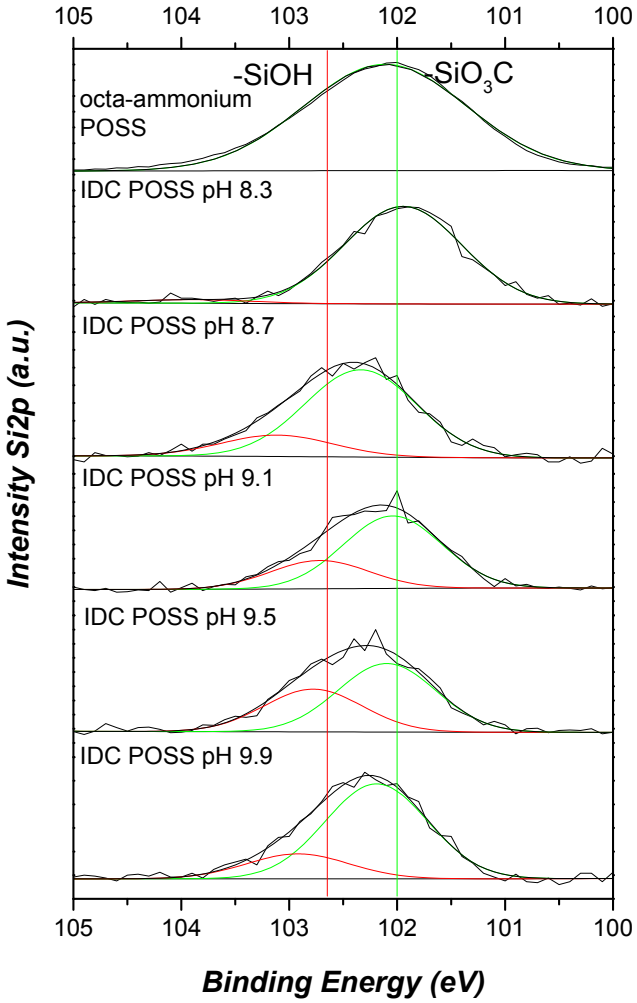

Figure 26: Comparison of XPS high resolution Si2p scans of octa-ammonium POSS and membranes synthesized at different pHs (pH 8.3, 8.7, 9.1, 9.5, 9.9; reaching from top to bottom). The octa-ammonium POSS spectrum identifies peaks at 102.11 eV associated with Si-O_3C (–) groups. In the polyPOSS amide spectra additional peaks at 103.2 eV emerge which are associated with the Si-OH (–) bonds from hydrolyzed POSS cages. The chemical shift of ~0.2 eV between the polyPOSS amide and octa-ammonium POSS spectrum results from the use of different XPS analysis equipment.

High Resolution Scan O1s

Figure 27 shows the comparison of XPS O1s peaks of octa-ammonium POSS and membranes synthesized at different pHs. The octa-ammonium POSS spectrum identifies peaks at 532.1 eV associated with siloxane group (Si-O-Si). In the polyPOSS-amide spectra an additional peak at 531.3 eV emerges ascribed to the amide group (NCO). From low to high synthesis pH the amide peak emerges, rationalized by the increasing Cross-linking of POSS cages with increasing pH. The chemical shift of ~0.2 eV between peaks of the polyPOSS-amide and octa-ammonium POSS spectrum results from the use of different XPS analysis equipment. A quantitative analysis of cross-linked POSS groups is not suitable since the program was not able to fit the hydrolysis peak of the POSS cages (Si-O*H).

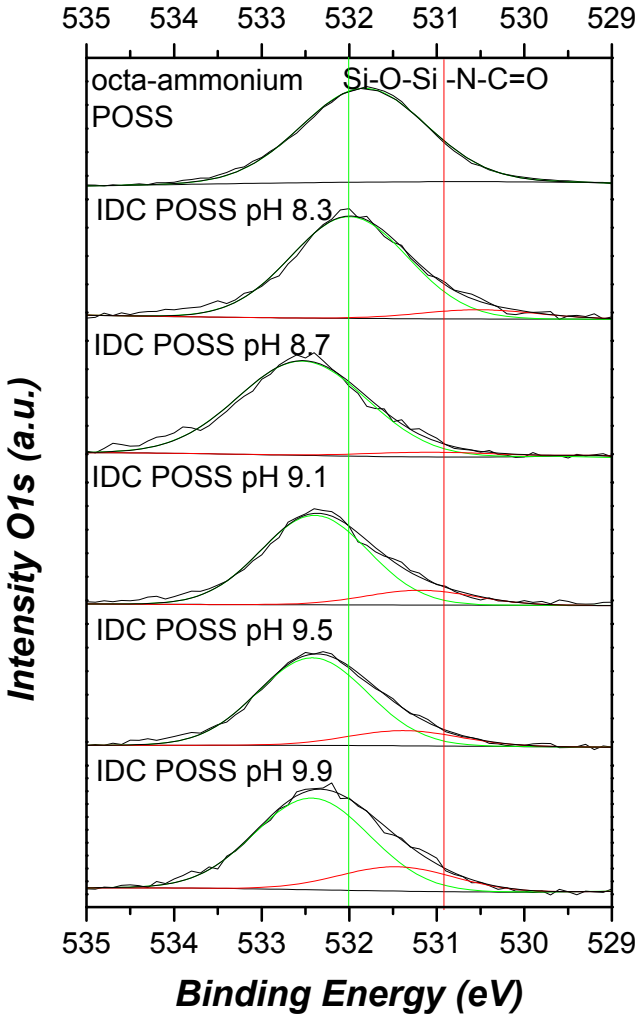

Figure 27: Comparison of XPS high resolution O1s scans of octa-ammonium POSS and membranes synthesized at different pHs (pH 8.3, 8.7, 9.1, 9.5, 9.9; reaching from top to bottom). The octa-ammonium POSS spectrum identifies peaks at 532.1 eV associated with siloxane group (Si-O-Si –). In the polyposs-amide spectra an additional peak at 531.3 eV emerges ascribed to the amide group (NCO –). The chemical shift of ~0.2 eV between peaks of the polyPOSS amide and octa-ammonium POSS spectrum results from the use of different XPS analysis equipment.

Elemental Ratio of Carbon and Silicon

Figure 28 shows the elemental ratio of carbon to silicon as a function of the synthesis pH of membrane. A general increase of the elemental ratio comparable with the analysis of the peak ratios of C-C to C-Si is observed. The increment is associated with a higher of cross linking with increasing preparation pH of membranes. This is because silicon and carbon intensities should decrease and increase as a function of synthesis pH, respectively. The trend-breaker of the IDC POSS membrane synthesized at pH 8.7 was already observed in previous XPS analysis. The deviation from the general trend is most likely due to contaminations.

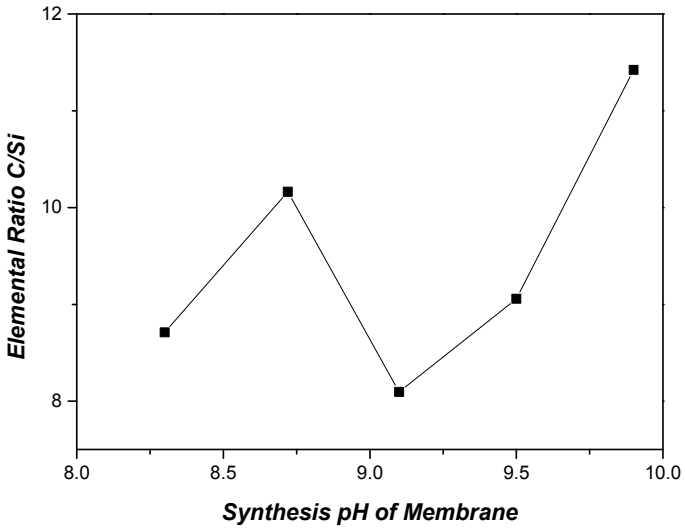

Figure 28: Elemental ratio of carbon to silicon as a function of the synthesis pH of IDC POSS membranes.

APPENDIX D- STREAMING ZETA POTENTIAL

Figure 29 shows the zeta potential for the IDC POSS membrane prepared at pH 9.5 by Evelien Maaskant on 7/3/2014 including error bars (95 % CI) as a function of titration solution. The data shows a net zero charge around pH 8. This might indicate that the membrane sample synthesized at pH 9.5 at 21/4/2014 possesses an exceptionally high IEP of pH 8.7. On the other hand it suggests that the reproducibility of IDC POSS membranes might be poor.

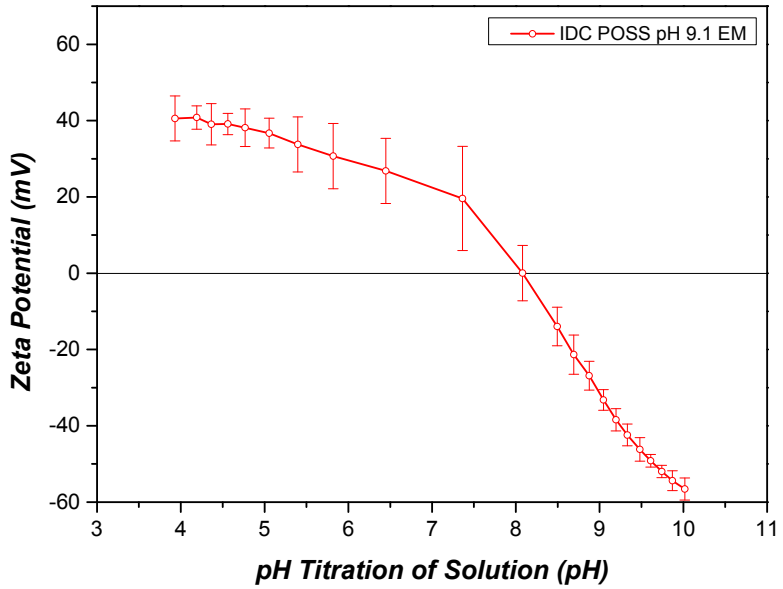

Figure 29: Zeta potential for IDC POSS membrane synthesized at pH 9.5 on 7/3/2014 including error bars (95% CI) as a function of pH of the titration solution.

Figure 30 shows the zeta potential in neutral pH environment (pH 7) as a function of the synthesis pH of the IDC POSS membranes. The figure indicates that all membranes are positively charged in neutral pH environment.

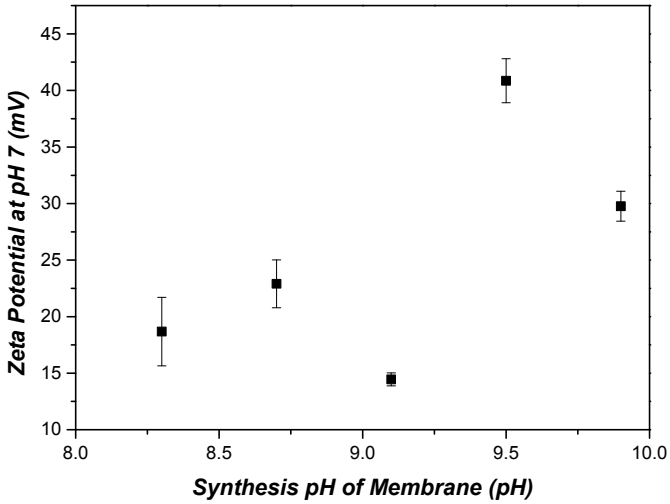

Figure 30: Zeta potential in neutral solution environment (pH 7) as a function of the synthesis pH of the IDC POSS membranes.

APPENDIX E- CONTACT ANGLE PH TITRATION

Figure 31 shows the contact angle for IDC POSS membranes synthesized at different pH values as a function of titration solution. The figure shows scattered data for all membranes and no trends are visible. The contact angles scatter from 85°-100°, suggesting a slightly hydrophobic nature of the IDC POSS membranes.

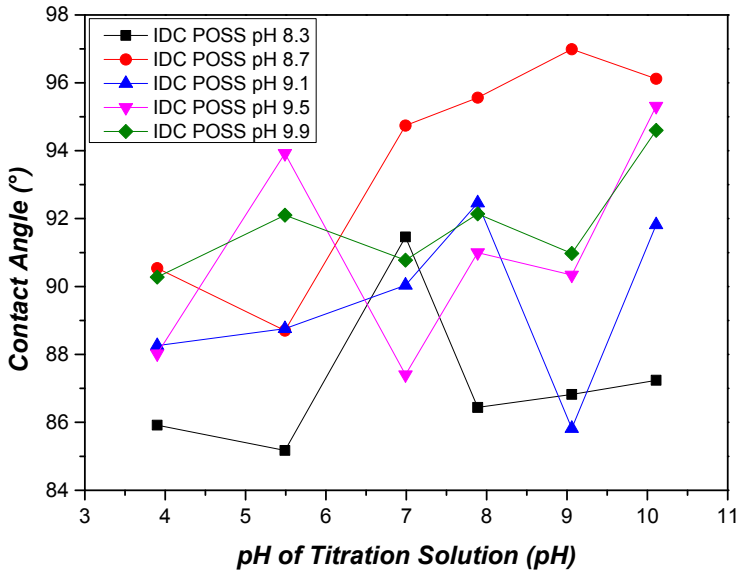

Figure 31: Contact angle pH titration for IDC POSS membranes synthesized at different pH values (pH 8.3 –, 8.7 –, 9.1 –, 9.5 –, 9.9 –) as a function of the pH of the different titration solutions.